Glycobiology vol. 19 no. 3 pp. 212–228, 2009
doi:10.1093/glycob/cwn101
Advance Access publication on October 2, 2008

Chemical and in situ characterization of macromolecular components of the cell walls from the green seaweed *Codium fragile*

José Manuel Estevez[2,3,4], Paula Virginia Fernández[5], Luciana Kasulin[5], Paul Dupree[6], and Marina Ciancia[1,3,5]

[4]Carnegie Institution of Washington, Plant Biology, Stanford University, Stanford, CA 94305, USA; [5]Cátedra de Química de Biomoléculas, Departamento de Biología Aplicada y Alimentos (CIHIDECAR-CONICET), Facultad de Agronomía, Universidad de Buenos Aires, Av. San Martín 4453, C1417DSE Buenos Aires, Argentina; and [6]Department of Biochemistry, University of Cambridge, Building O, Downing site, Cambridge, CB2 1QW, UK

Received on June 11, 2008; revised on September 15, 2008; accepted on September 29, 2008

A comprehensive analysis of the carbohydrate-containing macromolecules from the coencocytic green seaweed *Codium fragile* and their arrangement in the cell wall was carried out. Cell walls in this seaweed are highly complex structures composed of 31% (w/w) of linear (1→4)-β-D-mannans, 9% (w/w) of pyruvylated arabinogalactan sulfates (pAGS), and low amounts of hydroxyproline rich-glycoprotein epitopes (HRGP). In situ chemical imaging by synchrotron radiation Fourier transform infrared (SR-FTIR) microspectroscopy and by immunolabeling using antibodies against specific cell wall carbohydrate epitopes revealed that β-D-mannans and pAGS are placed in the middle part of the cell wall, whereas HRGP epitopes (arabinogalactan proteins (AGPs) and extensins) are located on the wall boundaries, especially in the utricle apical zone. pAGS are sulfated at C-2 and/or C-4 of the 3-linked β-L-arabinopyranose units and at C-4 and/or C-6 of the 3-linked β-D-galactopyranose residues. In addition, high levels of ketals of pyruvic acid were found mainly at 3,4- of some terminal β-D-Gal*p* units forming a five-membered ring. Ramification was found at some C-6 of the 3-linked β-D-Gal*p* units. In agreement with the immunolabeled AGP epitopes, a nonsulfated branched furanosidic arabinan with 5-linked α-L-Ara*f*, 3,5-linked α-L-Ara*f*, and terminal α-L-Ara*f* units and a nonsulfated galactan structure composed of 3-(3,6)-linked β-D-Gal*p* residues, both typical of type-II AG glycans were found, suggesting that AGP structures are present at low levels in the cell walls of this seaweed. Based on this study, it is starting to emerge that *Codium* has developed unique cell wall architecture, when compared, not only with that of vascular plants, but also with other related green seaweeds and algae.

Keywords: β-mannan/*Codium* cell wall/green seaweed/HRGP epitope/pyruvylated arabinogalactan sulfate

Introduction

Plant cell walls, in a broad sense, are complex multifunctional structures comprising different macromolecule types: (i) fibrillar or skeletal polysaccharide scaffolds (β-glycans), as cellulose, mannans, xylans, xyloglucans, arabinoxylans, mixed glucans, etc.; (ii) matrix-polysaccharides and proteoglycans including pectins, arabinogalactan proteins (AGPs), etc.; (iii) structural (glyco) proteins (i.e., extensins, etc.); (iv) phenolics and lignin-related compounds usually associated with secondary cell wall development. Despite the extensive knowledge of the chemical structure of the wall polymers, their interactions when they are assembled into the cell wall architecture remain elusive for most groups of plants.

The understanding of the spatial arrangement of the cell wall components is a considerable challenge that, at present, can be partially achieved using the different analytical techniques available. The use of in situ methods, such as the current library of monoclonal antibodies and carbohydrates binding modules (CBMs) against several cell wall carbohydrate epitopes (Moller et al. 2007), together with the noninvasive Fourier transform infrared spectroscopy coupled to a microscope (FTIR microspectroscopy), allows us to perform chemical imaging in plant cells and consequently, reveals intrinsic heterogeneities in a single cell wall or in many different cell wall types within a tissue (Carpita et al. 2001; McCartney et al. 2006). These in situ techniques are more powerful if complemented with chemical techniques, such as linkage analyses and spectroscopic methods (NMR, FTIR, etc.), that can be applied to isolated cell wall components (Moller et al. 2007).

Green seaweeds from Dasycladales and Bryopsidales groups including *Codium* are called "giant-cell" algae because their habits comprise continuous multinucleated siphons lacking cross cell walls and cell plate formation, unless at the septa formed in the basal part of reproductive structures (Figure 1A and B). *Codium fragile* (Suringar) Hariot is characterized by a cylindrical frond (Figure 1A) with a complex interwoven multiaxial siphon pattern comprising filaments with a coencocytic structure and enlarged utricles in their tips (Figure 1B). Cell walls of many green algal groups remain uncharacterized, with the exception of the glycoprotein-rich volvocacean walls (Ender et al. 2002; Hallmann 2006). It has been found that (1→4)-β-D-mannans are the predominant skeletal wall polymers in several genera of green algae, including *Acetabularia* (Dasycladales) and *Codium* (Bryopsidales) (Mackie and Sellen 1969; Chanzy et al. 1984; Ciancia et al. 2007; Dunn et al. 2007). However, (1→4)-β-D-mannans in these cell walls have been

[1]To whom correspondence should be addressed: Tel/Fax: +54-11-4524-8088; e-mail: ciancia@agro.uba.ar
[2]Present address: Departamento de Fisiología, Biología Molecular y Celular, Facultad de Ciencias Exactas y Naturales, Universidad de Buenos Aires, Ciudad Universitaria – Pabellón 2, 1428 Buenos Aires, Argentina.
[3]Research member of the National Research Council of Argentina (CONICET).

© The Author 2008. Published by Oxford University Press. All rights reserved. For permissions, please e-mail: journals.permissions@oxfordjournals.org

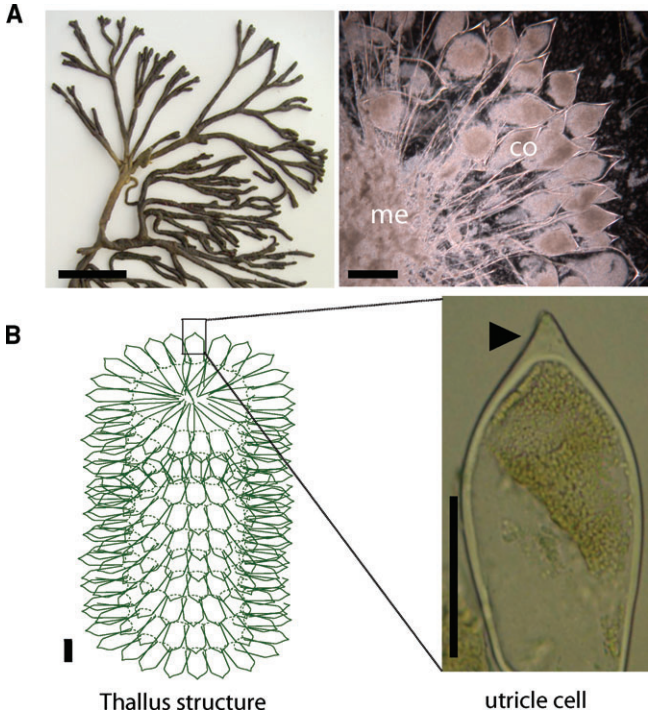

Fig. 1. Morphology of the coencocytic green seaweed *Codium fragile*. (**A**) General aspect of the dichotomous branched pattern in *C. fragile* (right). Scale bar = 1 cm. In addition, the inner structure of the thallus (right). Scale bar = 250 μm. (**B**) Schematic structure of the thallus structure (left) with the utricle view in detail (right, scale bar = 250 μm). Co = photosynthetic cortex; Me = medullar region. *C. fragile* has a mucron structure at the apical zone of the utricles (pointed tips, arrow). Scale bar = 40 μm.

poorly characterized compared with cellulose. If (1→4)-β-D-mannans were substituted to even a small extent, then these side chains would hinder their ability to form high tensile strength microfibrils, but might enhance their ability to form a flexible network (Dunn et al. 2007). Here we address if mannans in *C. fragile* have any detectable level of side chains and their precise in situ localization in the cell walls.

Matrix cell wall polysaccharides from green seaweeds (Percival and McDowell 1981) were classified into two main groups: (i) sulfated glucuronoxylorhamnans and glucuronoxylorhamnogalactans and (ii) sulfated xyloarabinogalactans. Polysaccharides from the genus *Codium* belong to the second group; however, a variable range of these polymers, from putative sulfated galactans and sulfated arabinans (or sulfated arabinogalactans) (Love and Percival 1964; Matsubara et al. 2001) to sulfated furanosidic (1→5)-α-L-arabinans (Uehara et al. 1992) and sulfated glucans (Matsubara et al. 2000), were partially described and some chemical evidence about their structures was informed. On the other hand, a highly pyruvylated galactan sulfate from *C. yezoense* was fully characterized (Bilan et al. 2007), and it was shown that the polysaccharide backbone is similar in many respects to (1→3, 1→6)-galactans of terrestrial plants present usually as type II-arabinogalactans; sulfate groups were found mainly at C-4, but also at C-6 of some of the β-D-galactose units and pyruvate was forming a five-membered ketal with O-3 and O-4 of nonreducing terminal galactose residues. In addition, recently two fractions were isolated from *Codium isthmocladum* showing a predominant linear 4-sulfated (1→3)-galactan structure with some units glycosylated or sulfated at C-6 (Farias et al. 2008).

In a previous paper, water-soluble polysaccharides from *C. fragile* and *Codium vermilara* were characterized (Ciancia et al. 2007). Both of them comprised a mixture of sulfated arabinans and galactans (or arabinogalactans). The galactan moiety had structural features similar to those of *Codium yezoense* and *C. isthmocladum*. The arabinan part was constituted by 3-linked arabinopyranose residues sulfated on C-2 and/or C-4. In addition, a β-D-mannan with a possible small degree of ramification (the side chains were clear for *C. vermilara*) was also obtained by water extraction and analyzed.

Arabinogalactans from *Codium* seem to be similar in many respects to (1→3, 1→6)-galactans of terrestrial plants present usually as type-II arabinogalactans, present in both pectins and AGPs. AGPs belong to a large group of cell wall proteoglycans and glycoproteins known as hydroxyproline-rich glycoproteins (HRGPs) (Gaspar et al. 2001; Showalter 2001). The main AGP-glycans structure consists of (1→3)-β-D-galactan chain partially substituted at C-6 by side chains of (1→6)-β-D-galactopyranose units, which often terminate in α-L-arabinofuranosyl residues; other sugars are commonly found in some AGPs (Nothnagel 1997; Tan et al. 2003). These *O*-glycoproteins are defined by postranslational modifications that include the hydroxylation of some proline residues (Yuasa et al. 2005) and the *O*-glycosylation of 4-hydroxyproline (Hyp) with complex AGs (Lamport 1965; Tan et al. 2003; Estevez et al. 2006). Hyp *O*-glycosylation type, restricted only to green algae and plants that shared a common algal ancestor in deep antiquity, is well described by the "Hyp-contiguity hypothesis" which predicts that the glycan addition in HRGPs is under the control of the protein primary sequence (Kieliszewski et al. 1992, 1995; Shpak et al. 1999). Regions of contiguous Hyp-residues [Ser-$(Hyp)_{n = 2–4}$] are typically glycosylated with arabinosides like in the extensins group, whereas larger type-II arabinogalactan *O*-glycans occur mainly on clustered, noncontiguous Hyp residues (X-Hyp-X-Hyp) such as in AGPs. These *O*-glycosylation patterns have been experimentally confirmed in several cases by expressing genetically encoded peptides (GEP) with AGP and extensin motifs in *Arabidopsis* and tobacco (Shpak et al. 1999, 2001; Kieliszewski 2001; Estevez et al. 2006; Lamport et al. 2006). The protein moiety is usually rich also in alanine, threonine, serine, and glycine residues (Nothnagel 1997). Although HRGPs are the major Hyp *O*-linked glycoproteins expressed throughout the plant kingdom (Lamport and Miller 1971; Kieliszewski, de Zacks et al. 1992; Showalter 2001; Ender et al. 2002; Estevez, Leonardi, et al. 2008), there is no report until present describing AGPs or extensins in the cell walls of any kind of seaweed.

In this article, we have characterized the complex cell walls from the green seaweed *C. fragile* (Suringar) Hariot in terms of their polymer composition and their in situ localization. Three main cell wall carbohydrate polymeric components were found: (i) major amounts of (1→4)-β-D-mannans as the main structural cell wall polysaccharides; (ii) intermediate quantities of pyruvylated arabinogalactan sulfates (pAGS); and (iii) low amounts of HRGP epitopes of the AGPs and extensin type. This work is the initial study of the cell wall polymers structure and arrangement in *Codium*, including the comparison with those of green algae and land plants, in order to provide insights into the unique cell wall architecture of these seaweeds.

Results

To characterize the cell walls from *C. fragile*, polymers were obtained (Figure 2A) by successive extractions with water at room temperature (RT) (A1–A2, composed mostly of sulfated polysaccharides) and at 90°C (M1–M2, mannan-enriched fractions), which were partially characterized elsewhere (Ciancia et al. 2007). The residue from the water extractions (RM2, Table S1) was composed of 18% of proteins and 70% of carbohydrates, mainly mannose, but a small amount of sulfated arabinogalactans (7–8%) was still present.

(1→4)-β-D-Mannans as major structural cell wall polysaccharide

A mannose-rich polymer (Figure 2A), partially extracted with hot water (extracts M1–M2), was the major component in the residue RM2, which comprises 43% (w/w) of the dry seaweed (Table S1). The FTIR spectrum of RM2 (Figure 2B) showed unique bands similar to those reported for (1→4)-β-D-mannans (Dunn et al. 2007). Accordingly, the band at 1151 cm^{-1} was assigned to the glycosidic C–O–C vibration of (1→4)-β-D-mannans, whereas the peaks at 1061 and 1032 cm^{-1} were associated with C–O–C and C–C bonds of mannose unit rings, respectively (Dunn et al. 2007). Mannans with repetitive (1→4)-β-linkages were found previously by linkage analysis of extracts M1/M2 in *C. fragile*; the presence of side chains was not confirmed. However, the possible side chains on the main backbone were detected for a mannan obtained from a related species, *C. vermilara* (Ciancia et al. 2007). To determine if mannans from *C. fragile* have a (1→4)-β-D-mannosyl repetitive linear structure, or if there is any substitution or side chain, the RM2 cell wall fraction was submitted to an enzymatic hydrolysis with a specific mannanase that hydrolyzes only (1→4)-β-D-mannosyl units. The product released (RM2dig), where mannose was the major monosaccharide (Glc + Gal < 0.5%), was analyzed by carbohydrate gel electrophoresis (PACE) (Figure 2C). The main products from RM2dig were mannobiose, mannotriose, mannotetraose, and mannose that migrate exactly as those derived from the commercial (1→4)-β-D-mannan (Figure 2C).

The mannosyl-oligosaccharide fraction (RM2dig) was analyzed by linkage and 2D NMR analyses (Figure 2D). Linkage analysis clearly showed 37 mol% *t*-Man units at the nonreducing end and 63 mol% of 4-linked Man, no evidence of disubstituted mannose units was found. In agreement with the linkage analysis, the HSQC spectrum showed four groups of δ_H/δ_C correlations in the anomeric region (Figure 2D). In the first group, at least two signals at δ_H/δ_C 4.62/100.5 and 4.65/100.2 correspond to 4-linked β-D-mannosyl units: the first one corresponds to these units linked to the nonreducing end unit and the second one linked to another 4-linked mannosyl unit. The signal at δ_H/δ_C 4.74/99.4 was assigned to β-D-mannosyl units at the nonreducing end of the (1→4)-β-D-backbone, and those signals at δ_H/δ_C 5.07/94.0 and 4.80/93.9 correspond to α- and β-terminal reducing ends of 4-linked mannosyl units, respectively. In addition, two strong signals at δ_H/δ_C 3.72/77.5 and 3.68/77.5 correspond to C-4/H-4 of both substituted 4-linked β-D-Man*p* units (Davis et al. 1995). Moreover, in the HMBC experiment (not shown) the β-1→4 linkages in the mannosyl backbone were confirmed by the strong correlations between H-1 of the nonreducing end unit and C-4 of the mannose residue linked to the nonreducing end and the interlink unit (δ_H/δ_C 4.74/77.5) and between H-4/C-1 (δ_H/δ_C 3.74/100.4 and 3.8/100.4, respectively). Based on these results, it was confirmed that the fibrillar mannan from *C. fragile* has a linear structure of (1→4)-β-D-mannan backbone with no side chains in detectable levels.

Cell walls at the utricle tip from *C. fragile* were mapped using SR-FTIR microspectroscopy. The in situ distribution intensities of the main absorbances at 1151, 1092, 1061, and 1032 cm^{-1} that correspond to (1→4)-β-D-mannan polymer are shown in Figure 3A. Clearly, absorbance intensities of mannan-associated bands increased drastically from the boundaries toward the center of mucron cell wall area (Figure S1). In agreement with that, birefringence (PC), Calcolfluor White staining (CW), and finally, antibody labeling with anti-mannan mAb (Mab, Table 2S) showed a similar (1→4)-β-D-mannan localization pattern (Figure 3B). In addition, an in situ enzymatic treatment using the same mannanase as before was performed on seaweed cross-sections. The amount of mannose units released after enzymatic degradation (Figure 3C) was 7-fold higher in the mannanase-treated cross-sections than in the negative control. Cell wall CW-staining (CW β-ManT) in the treated sections was very low or undetectable in comparison with the control (Figure 3D) confirming the pattern of (1→4)-β-D-mannan distribution.

Pyruvylated arabinogalactan sulfates

Preliminary structural analysis of extract A1 isolated from *C. fragile* (Table I, Figure 2A) indicated the occurrence of a pyruvylated arabinogalactan sulfate (pAGS) or a mixture of sulfated arabinans (AS) and pyruvylated galactan sulfates (pGS) (Ciancia et al. 2007). In this study, a high content of sulfate was also detected by the FTIR analysis (Figure 4A), where strong bands at 1384 cm^{-1} (common for all sulfate esters) and at 1250–1230 cm^{-1} (asymmetric stretching of the O=S=O) were present. Additional bands at 850 cm^{-1} (C–O–S, secondary axial sulfate) and at 820 cm^{-1} (C–O–S, primary sulfate) indicate that some of the sulfate groups are located at C-4 and C-6 of the D-galactose residues, respectively (Prado Fernández et al. 2003) (Figure 4A). The bands for sulfate groups of the Ara*p* units are possibly overlapped in the 820–850 cm^{-1} region (see structural analysis, Table II). In addition, the band at 1427 cm^{-1} would correspond to the carboxylic group of the pyruvic acid (Prado Fernández et al. 2003). Accordingly, sulfate groups of the pAGS were labeled with toluidine blue *O* (TB*O*) at pH = 1 and also with ruthenium red (RR) that reacts with polyanions (Krishnamurthy 1999) mostly in tip of the mucron area and also close to the plasmamembrane (Figure 4B). RR would react not only with the sulfate groups, but also with the carboxylate groups of the pyruvic acid present in the pAGS polymers.

A1 was analyzed by ion-exchange chromatography (IEC, Figure 4C) in order to address its structural dispersion. An important part of the sample, F1 (71% w/w of the recovered material) with similar characteristics to the original product, although less sulfated (Table I) and more pyruvylated (Gal:pyruvate molar ratio of ∼ 4:1, Table I), was obtained in the fraction eluted with water. A further step of purification by IEC of F1 (not shown) gave one major fraction obtained at 4 M NaCl (92.5% w/w), containing mostly galactose and arabinose units with a molar ratio of ∼1:0.5. In addition, one minor fraction was eluted at 2 M NaCl (7.5% w/w) that contained mostly galactose (not shown). These results suggest that, even though A1/F1 could be composed of more than one glycan structure,

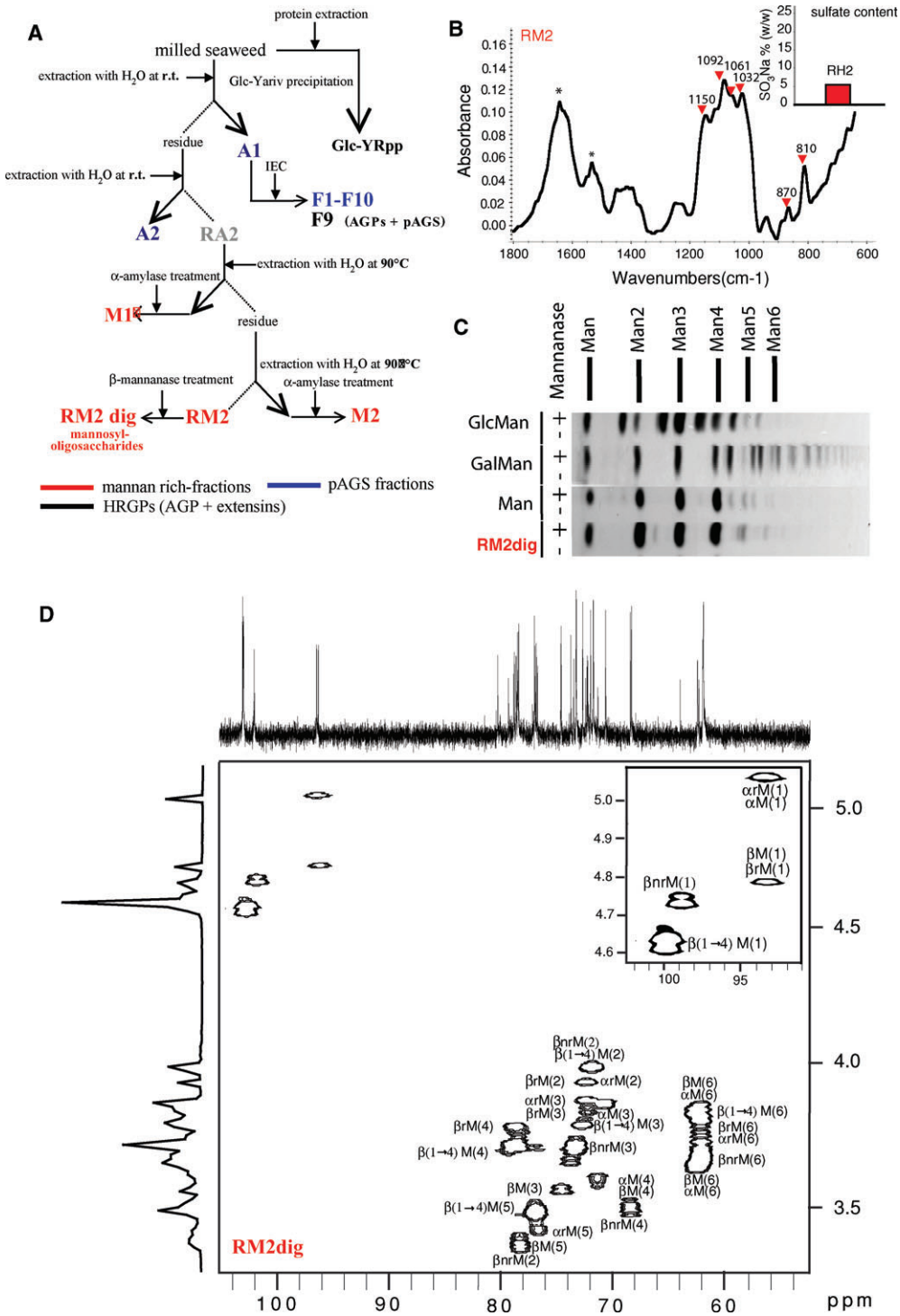

Fig. 2. Cell wall polymer extraction and purification (top). Characterization of (1→4)-β-D-mannans from cell walls. (**A**) Flowchart extraction and isolation of the different cell wall polymers obtained from *C. fragile*. (i) Extraction with water at room temperature (mostly sulfated polysaccharides in fractions A1 and A2). (ii) Extraction with water at 90°C (mannose-rich fractions M1 and M2). (iii) Buffer extraction and β-Glc-Yariv precipitation of AGPs (Glc-Yariv precipitate, β-Glc-Yariv- pp). (iv) In addition, A1 was analyzed by ion-exchange chromatography (IEC) and F1–F10 were obtained. Only F1, F6, and F9 were studied in detail. In order to characterize the structure of the mannans, the residue from the hot water extraction (RM2) was treated with β-mannanase and manno-oligosaccharides (RM2dig) were isolated and characterized. (**B**) FT-IR spectrum of RM2. Peaks of interest are indicated on the FTIR spectra with arrows for those corresponding to β-mannans (1151, 1092, 1061, and 1032 cm^{-1}) and with asterisks (*) for those corresponding to proteins (1650 and 1540 cm^{-1} for amide I and II bands, respectively). On the top left, sulfate content on dry weight basis for RM2. (**C**) Algal cell wall-manno-oligosaccharides derived from RM2 (RM2dig) were compared by PACE with ivory nut manno-oligosaccharides, Konjac glucomanno-oligosaccharides and locust bean galactomanno-oligosaccharides, obtained using the endomannanase Man5A.The main products of the digestion of RM2 were mannose, mannobiose, mannotriose, and mannotetraose. Oligosaccharides released from digestion of 1.25 μg cell wall or 0.5 μg standard polysaccharides are shown. (**D**) HMBC spectra of the manno-oligosaccharides. The following units are shown in the spectra: nrM(1→ (nonreducing end units), β-(1→4)-M (units present in the 1→4 backbone), β/αrM (reducing end units), and β/αM (closest units next to the nonreducing end units).

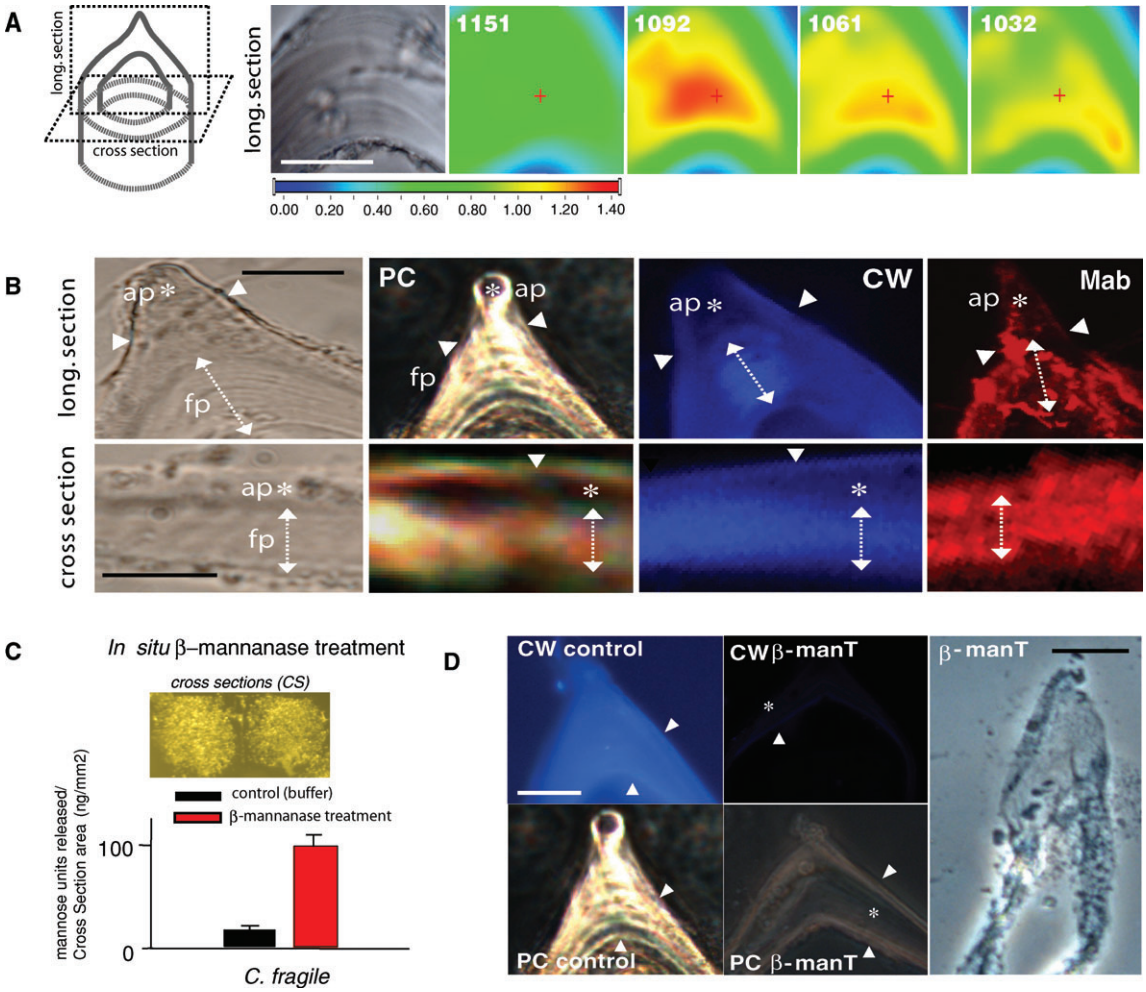

Fig. 3. In situ distribution of (1→4)-β-D-mannans in *C. fragile* cell walls. (**A**) Chemical images using SR-FTIR microspectroscopy of the cell wall in a longitudinal section view from the mucron tip. A cell wall area of 80 × 60 μm was mapped with a 10 × 10 μm window resolution. FTIR-maps with relative absorbance intensities corresponding to characteristic peaks belonging to β-(1→4)-D-mannans (1151, 1092, 1061, and 1032 cm^{-1}) are shown. The color gradient used in the chemical images is shown below. (**B**) Fibrillar-like (fp, double arrows) and amorphous-like phases (ap) of the cell wall from the utricle tip (mucron, on top) and utricle side (bottom), both in a longitudinal view observed with transmitted light (left), phase contrast microscopy (PC), Calcoflour White-staining (CW), and (1→4)-β-D-mannan labeling (anti-mannan antibody, Mab, right; Handford et al. 2003). Scale bar = 40 μm. (**C**) In situ mannanase-treatment of *Codium* cell walls. Mannose units released per cross-section (CS) area of the thallus after in situ β-mannanase treatment (ng mannose mm^{-2}) compared with buffer incubation used as a control (left). Forty cross-sections were used for each treatment. (**D**) Utricle cell wall (on the top) before (CW-control) and after β-mannanase treatment (CW-β-manT). Cell wall observed before (PC-control) and after β-mannanase treatment (PC-β-manT) using phase contrast microscopy (PC) to enhance the arrangement of linear (1→4)-β-D-mannans (bottom). Almost, the complete absence of CW staining and very low birefringence of walls is observed after β-manT causing cell wall disruption in some areas (left). Scale bar = 40 μm.

Table I. Yields and analyses of the fractions obtained from A1 by ion-exchange chromatography (IEC) on Sephadex DEAE A-25

Fraction[a,b,c]	Eluent solvent (M, NaCl)	Yield (%)	Carbohydrates (%)	Sulfate as SO_3Na (%)	Proteins (%)	Monosaccharide composition (mol%)					
						D-Gal	L-Ara	D-Man	D-AnGal	D-Xyl	D-Glc
A1[d]	–	6.7	50.5	20.6	11.3	61.6	23.1	3.9	2.0	3.2	4.8
AG-fraction											
F1	0.0	42.6	33.4	12.2	10.5	65.2	22.4	2.1	Tr	1.4	7.3
GaL-rich fractions											
F6	1.0	3.3	41.5	11.0	Tr	84.8	2.5	1.2	4.3	2.5	3.2
F7	1.5	4.2	44.1	19.4	Tr	87.1	12.9	Tr	–	Tr	Tr
Ara/Gal-rich fractions											
F8	2.0	2.5	36.6	24.2	Tr	43.5	50.8	–	–	1.9	1.5
F9	3.0	3.6	31.6	25.5	Tr	60.7	37.3	Tr	Tr	Tr	2.0

[a]Traces of 2-Gal, 6-Gal, Fuc, and Rham were detected in most of the fractions.
[b]AG = arabinogalactan; Tr = traces.
[c]Analysis of the fractions F2–F5 and F10 was not included in this table because of their low yields (≤1.0% w/w).
[d]From Ciancia et al. (2007). Included for comparison.

still the main component is a pAGS polysaccharide. The unexpected behavior of A1/F1 by IEC would be related with the capacity of these samples to form aggregates, possibly, mediated by important amounts of divalent cations (Ca^{2+} and Mg^{2+}; Ciancia et al. 2007), that preclude the sulfate groups interaction with the resin. After the first IEC and F1 workup, this effect would be lost and the sample is strongly retained by the anion exchange phase and only released with a highly concentrated NaCl solution.

Linkage analysis of A1 (Ciancia et al. 2007) together with that of the corresponding desulfated product (DsA1, this study) showed that sulfate groups were located in the following positions: (i) 2,4- (15%) and 4- (10%) of the 3-linked β-L-Ara*p* units and (ii) 4,6- (7%), 4- (3%), and 6- (7%) of the 3-linked β-D-Gal*p* residues (Table II). In addition, the presence of pyruvylated units (Gal:pyruvate molar ratio of ∼ 4:1) was confirmed mainly as terminal β-D-Gal*p* units pyruvylated at position 3,4- (18%), but minor amounts of pyruvic acid at 4,6- of the 3-linked β-D-Gal*p* units were also found (see below NMR analysis). In addition, 14% of 3-linked β-D-Gal*p* would be substituted on C-6 and sulfated on C-4. On the other hand, characteristic type-II AG linkages with 9% of 3-linked β-D-Gal*p* and 6% of 3,6-linked β-D-Gal*p* were also detected (Table II).

Linkage analysis of F1 and its corresponding desulfated product (DsF1) gave similar results to those of A1, although a higher amount of 3-linked β-D-Gal*p* (19%) and 3,6-linked β-D-Gal*p* (18%) units were found (Table II). The ^{13}C NMR spectra of A1 and F1 (Figure 5A, Table IV) showed in the anomeric region signals at 105.0–103.5 ppm, that correspond to the major β-D-Gal*p* units in different environments, as deduced from linkage analysis of (Ds)A1 and (Ds)F1. In the anomeric region of HSQC spectra, at least four groups of signals (δ_{H1}/δ_{C1}) corresponding to β-D-Gal*p* units with different substitutions were found (Table IV): (i) 4.75–4.65/105.0–103.5 ppm and (ii) 4.55–4.45/105–103 ppm, the first one corresponding to β-D-galactose residues linked to C-3 of another unit, while the second is due to the same units, but linked to C-6 of another unit (Bilan et al. 2007). Important amounts of 4-sulfated, 3- and 3,6-linked β-D-galactose units were confirmed by the presence of important signals at δ_H/δ_C 4.80–2/78.1 and 4.02–6/79.3 due to C-4 and C-3, respectively, of these units (Bilan et al. 2007). Besides, the presence of 3-linked, 6-sulfated β-D-galactopyranose units was verified by the signals at δ_H/δ_C 4.05 and 3.94/68.5 (Estevez et al. 2004). In addition, the HMBC spectra of A1/F1 correlations, corresponding to the (1→3) glycosidic linkages of the Gal*p* 4-sulfate (6-substituted) at δ_{H1}/δ_{C3} 4.84/78.1 and at δ_{H3}/δ_{C1} 4.02–8/104.5 and those corresponding for (1→6)-linkages at δ_{H1}/δ_{C6} 4.84/71.6 and at δ_{H6}/δ_{C1} 4.05/104.5 of the similar units, were detected. Moreover, (1→3) linkages of the nonsulfated Gal*p* units were also found at δ_{H1}/δ_{C3} at 4.68/83.3 and at δ_{H3}/δ_{C1} at 3.84/104.5 (not shown).

On the other hand, correlation peaks at δ_H/δ_C 1.61/108.5 and at 1.61/178.5 in the HMBC spectrum of A1 (the later was not detected in F1) show that the major methyl group belongs to a pyruvic acid (Figure 5B). The signals at δ_H/δ_C 1.61/24.3 in the HSQC spectra belong to the major methyl group in the pyruvic acid (Figure 5A). Based on these signals, we assigned a five-membered ketal cycle [3,4-*O*-(1′-carboxy)-ethylidene] of pyruvic acid in S configuration and linked mostly to terminal units of β-D-galactose. In addition, a weak correlation peak at δ_H/δ_C 1.47/26.1 corresponds to a minor methyl group. Moreover, the HMBC spectrum showed a weak correlation at δ_H/δ_C 1.47/101.9

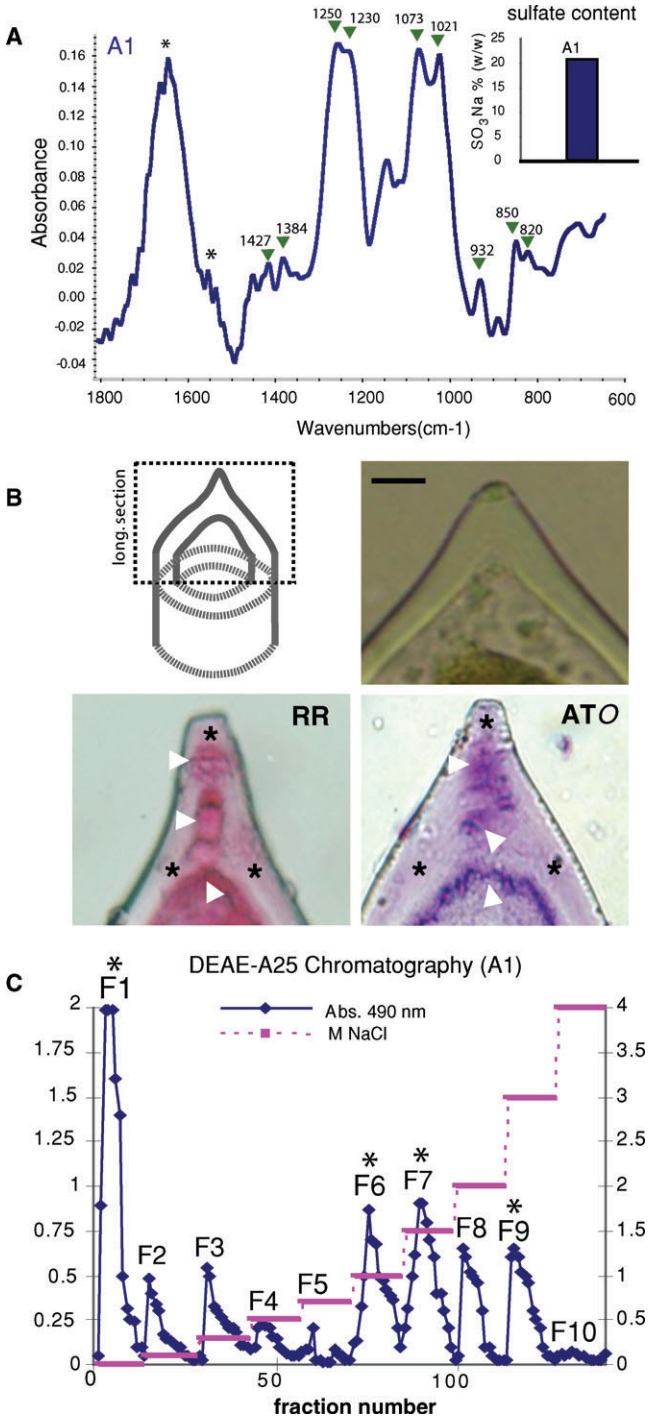

Fig. 4. Isolation and characterization of the pyruvylated arabinogalactan sulfates (pAGS). (**A**) FT-IR spectra of the highly sulfated extract A1 from *C. fragile*. Peaks of interest are indicated on the FTIR spectra (arrows) corresponding to sulfate groups (1384, 1250, 1230, and 850 cm^{-1}), proteins (*) (1650 and 1540 cm^{-1} for amide I and II bands, respectively), and those possibly associated with the pyruvylated arabinogalactan sulfate backbone (1073, 1021, and 932 cm^{-1}). In addition, the band at 1427 cm^{-1} would correspond to the carboxylic group of the pyruvic acid. On the top left, sulfate content on dry weight basis for A1 fraction. (**B**) Localization of anionic polysaccharides (ruthenium red, RR bottom left) and sulfated polysaccharides (toluidine blue *O* staining at pH = 1, TB*O*, bottom right) on the utricle cell tip. Scale bar = 40 μm. High-staining cell wall areas are indicated with arrowheads and the absence or low staining is shown with asterisks (*). (**C**) Ion-exchange chromatography (IEC) of the main extract A1 gives fractions F1–F10. Asterisks (*) correspond to those fractions that were analyzed in detail in this study.

Table II. Linkage analysis of the pyruvylated arabinogalactan sulfate **A1** and the major fractions isolated from **A1** (**F1** and **F6**) by IEC (Sephadex DEAE A-25) and the desulfated products obtained from them (**DsA1, DsF1**, and **DsF6**) (mol%)

Monosaccharide[a,b]	Structural unit[c]	**A1**[d]	**DsA1**	**F1**	**DsF1**	**F6**	**DsF6**
2,3,5-Ara	L-Ara*f*(1→	Tr[e]	–	Tr.	2	Tr	Tr
2,4-Ara	→3) L-Ara*p*(1→	–	**29**[f]	5	**19**	Tr	**3**
2-Ara	→3) L-Ara*p***4S**(1→ (mayor), →3,5) L-Ara*f*(1→ (minor)						
		10	1	5	Tr	Tr	–
4-Ara	→2,3) L-Ara*p*(1→	–	–	5	4	3	**1**
Ara	→3) L-Ara*p***2,4S**(1→	24	**9**	8	**–**	Tr	–
2,3,4,6-Gal	D-Gal*p*(1→	Tr	Tr	Tr	Tr	1	–
2-AG	→4) D-AnGal*p*(1→	–	–	–	–	4	–
2,4,6-Gal	→3) D-Gal*p*(1→	9	**20**	19	21	23	**26**
2,3,6-Gal	→4) D-Gal*p*(1→	1	–	1	–	Tr	–
2,6-Gal	3,4Pyr- D-Gal*p*(1→ (major)[6], →3) D-Gal*p***4S**(1→, and →3,4) D-Gal*p*(1→ (minor)	21[g]	22[g]	23[g]	**29**[g]	37	**32**
6-Gal	ND[h]	Tr.	Tr	Tr	1	Tr	2
2,3-Gal	→6) D-Gal*p***4S**(1→, →4) D-Gal*p***6S**(1→ or →4,6) D-Gal*p*(1→	3	–	Tr	Tr	3	3
2,4-Gal	→3) D-Gal*p***6S**(1→, →3,6) D-Gal*p*(1→	6	**14**	18	19	11	**18**
2-Gal	→3) D-Gal*p***4,6S**(1→, →3,6) D-Gal*p***4S**(1→, and →3) D-Gal*p*4,6-Pyr(1→ (minor)	23	**2**	15	**6**	19	**10**
3-(4-) Gal	ND	3	3	Tr	Tr	Tr	4

[a]Methyl groups at the positions indicated.
[b]Small amounts of Glc and Man derivatives were detected, but not included in this table.
[c]Sulfate groups are highlighted in order to aid in interpret this table.
[d]Data from Ciancia et al. (2007) were included for comparison.
[e]Tr = traces.
[f]Those values that have significantly changed in the desulfated derivatives in comparison with the original samples are highlighted.
[g]This value is in agreement with the galactose:pyruvic acid molar ratio of ∼4: 1 for A1/F1.
[h]ND = not defined.

and at 1.47/178.5 (Figure 5B), indicating the presence of galactose residues with 4,6-*O*-(1′-carboxy)-ethylidene cyclic ketals in R configuration as a minor component of the polysaccharide (Bilan et al. 2006). The proportion of about 20–22:1 between five- and six-membered ketals was calculated from ^{1}H NMR spectra of A1 and F1.

Anomeric ^{1}H–^{13}C signals at δ_H/δ_C 5.38/96.8, 5.45/94.8, 5.41/94.4, and 5.31/93.8 in A1 were assigned tentatively to 3-linked β-L-Ara*p* 2,4-disulfate units in two slightly different environments, 3-linked β-L-Ara*p* 4-sulfate residues, and possibly to 2,3-linked β-L-Ara*p* units, respectively (Table IV). These values indicate much protected C-1 for the corresponding units, as values usually found for these carbon atoms are around 105 and 101 ppm for α-L-arabinopyranosyl and β-L-arabinopyranosyl residues, respectively, in a polysaccharide chain (Bock et al. 1986). These assignments (Table IV) are in agreement with the linkage analysis (Table II).

Galactan-, arabinan-, and AGP structures as minor cell wall components

In order to obtain more information about the glycan structural dispersion of A1, one of the minor fractions isolated by IEC rich in galactose (F6) and one rich in arabinose (F9) was analyzed in detail (Tables I–III). Linkage analysis of F6 and its desulfated derivative (DsF6) showed that the main structure is a pyruvylated galactan sulfate (pGS) composed of 3-linked β-D-Gal*p* residues (23%) with sulfated groups on C-4 (5%) or substituted at C-4 and C-6 (10%) and 4,6-pyruvylated (∼1%, see later NMR). In addition, 3,6-linked β-D-Gal*p* (11%) units, partially sulfated on C-4 (9%), and terminal 3,4-pyruvylated β-D-Gal*p* residues (32%) were detected (Table II); signals present in the ^{13}C NMR spectrum of F6 (Figure 6A) were in agreement with results obtained by linkage analysis (Table II). The ratio of pyruvic acid forming a ketal ring with 3,4- of the terminal β-D-Gal*p* units and 4,6- of the 3-linked β-D-Gal*p* residues, respectively, was 17:1 from the ^{1}H NMR spectrum (from signals at δ_H 1.61 and 1.47, which correspond to the methyl groups, Figure 6A), very similar to that of A1/F1. The other signals corresponding to the methyl, carboxylic groups, and ketal carbon atoms of the five- and six-membered ketal cycles are the same as those described for A1/F1. Structural analysis of fractions F7 and F8 showed structures similar to those described above.

Surprisingly, a unique furanosic arabinosyl structure was detected in the arabinose-rich fraction F9. Linkage analysis of F9 (Table III) indicated the presence of terminal, 5-linked and 3,5-linked arabinofuranosyl residues. In concordance with these data, the ^{13}C NMR of F9 (Figure 6B) shows very clearly three sets of signals due to 5-linked, 3,5-linked, and terminal α-L-arabinofuranosyl residues (Table IV, Navarro et al. 2002; Dourado et al. 2006). These data show the presence of a 5-linked arabinan branched at C-3 as a major component of F9 (Figure 6C). In addition to that, 3-linked (∼10%) and 3,6-linked Gal*p* (<8%) units were also detected. Altogether, these results show the presence in the fraction F9 of AGP-like structures as well as pAGS (Table III) with similar characteristic to those described before for A1/F1. On the other hand, the presence of considerable quantities of nonpyruvylated terminal nonreducing galactose units (11%) and 4,6-disubstituted galactose residues (6%) that were not found in any other fraction is noteworthy.

The assignments of most of the NMR signals corresponding to the pAGS, pGS, and AGP-like structures isolated from *C. fragile* cell walls are shown in Table IV.

Cell wall AGP and extensin epitopes

Several evidences suggest that low amounts of cell wall glycoproteins of the HRGP type are present in the cell walls of *C. fragile*: (i) the detection of cell wall proteins by CB and SR-FTIR (see later Figure 7D); (ii) the occurrence of Hyp, together with

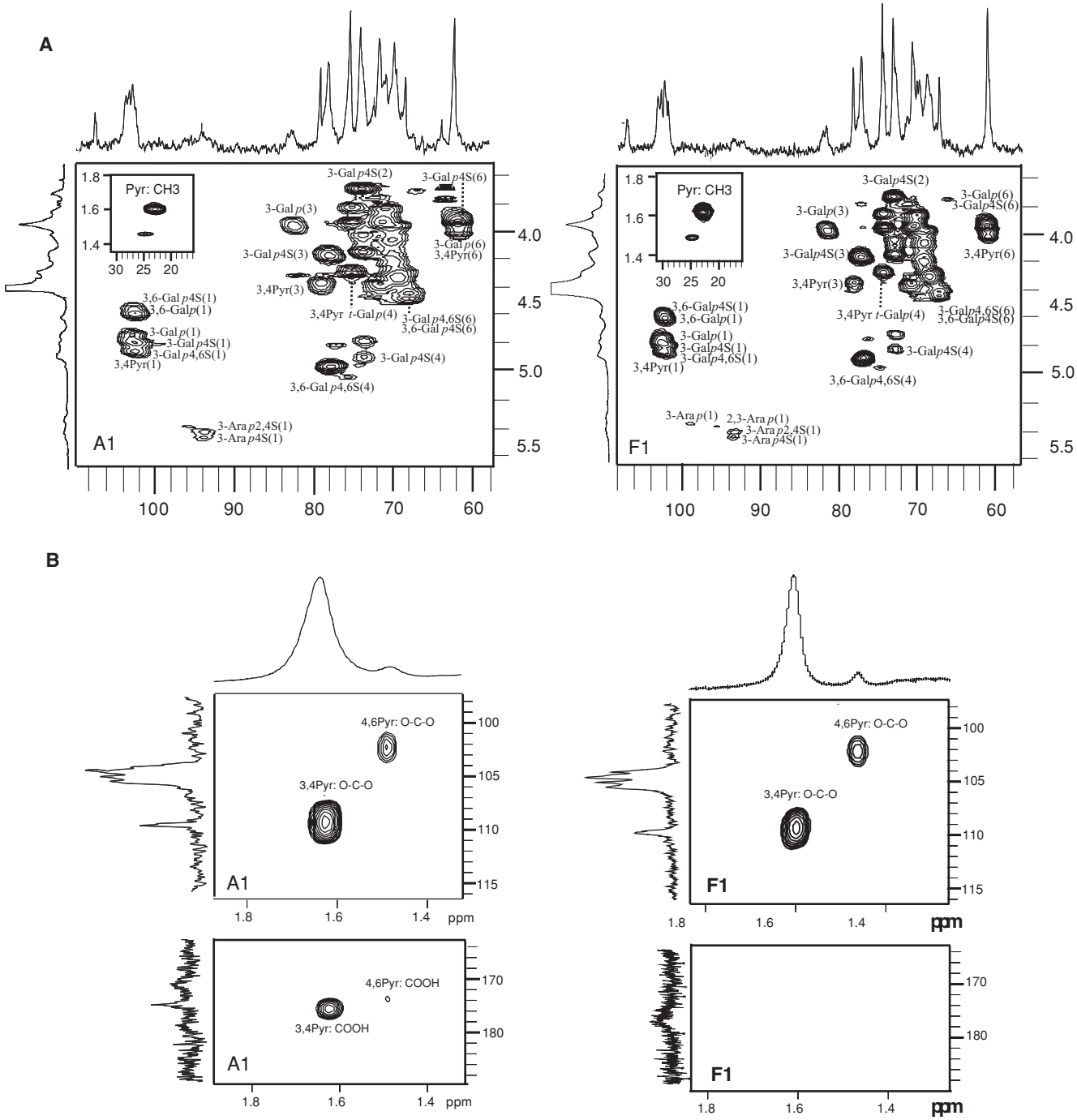

Fig. 5. 2D NMR characterization of the pyruvylated arabingalactan sulfate (pAGS). (**A**) HSQC spectrum of A1 and the major fraction F1 obtained by IEC. (**B**) A part of the 2D HMBC spectra of A1 and F1. Signals for CH_3 (δ_H/δ_C 1.61/24.3), O–C–O (δ_H/δ_C 1.61/108.5), and COOH groups (δ_H/δ_C 1.61/178.5) of the five-membered ketal cycle [3,4-*O*-(1′-carboxy)-ethylidene] of pyruvic acid ketals linked to terminal units of β-D-galactose are shown. In addition, weak correlations at δ_H/δ_C 1.47/26.1, 1.47/102.1, and at 1.47/178.5 indicate the presence of galactose residues substituted with 4,6-*O*-(1′-carboxy)-ethylidene cyclic ketals as a minor component of the polysaccharides A1/F1. See Table IV for NMR signal assignments.

other hydroxylated aminoacids, in the protein moiety (see Table S3); (iii) the presence of nonsulfated 3- and 3,6-linked β-D-Gal*p* units together with small amounts of 5-(3,5)- and terminal α-L-Ara*f* residues (Tables II; IV). These types of structural units are typically found in the glycan moiety of the AGP conjugates (Gane et al. 1995; Tan et al. 2003).

To test the presence of these putative HRGPs in *C. fragile*, a set of available antibodies against AGP and extensin structures (Table S2) was applied in an immuno dot-blot assay (IDA) on the cell wall extracts and residue (A1-M2 and RM2). Reaction against AGP epitopes (JIM-16 and MAC 207 mAbs, Pennell et al. 1989; Knox et al. 1991; Yates et al. 1996) and also against arabinosides of the extensin type (JIM-11 and JIM-20 mAbs, Smallwood et al. 1994) was strong mainly with A1, but they also bonded in lower extent to the other cell wall fractions (Figure S2). Therefore, A1 was analyzed by sodium

Table III. Linkage analysis of F9, minor arabinan-rich fraction isolated from **A1** by IEC (mol%)

Monosaccharide[a,b]	Deduced structural unit[c]	**F9**
2,3,5-Ara	L-Ara*f*(1→	**12**[d]
2,3-Ara	→5) L-Ara*f*(1→	**11**[d]
2-Ara	→3,5) L-Ara*f*(1→	**4**[d]
2,4-Ara	→3) L-Ara*p*(1→	10
4-Ara	→2,3) L-Ara*p*(1→	4
Ara	→3) L-Ara*p***2,4S**(1→	2
2,3,4,6-Gal	D-Gal*p*(1→	**11**[d]
2,4,6-Gal	→3) D-Gal*p*(1→	**10**[d]
2,3,6-Gal	→4) D-Gal*p*(1→	1
2,6-Gal	3,4Pyr- D-Gal*p*(1→ (major), →3) D-Gal*p***4S**(1→, and →3,4) D-Gal*p*(1→ (minor)	9
2,3-Gal	→4) D-Gal*p***6S**(1→ or →4,6) D-Gal*p*(1→	6
2,4-Gal	→3) D-Gal*p***6S**(1→, →3,6) D-Gal*p*(1→	**8**[d]
2-Gal	→3) D-Gal*p***4,6S**(1→, →3,6) D-Gal*p***4S**(1→, and →3) D-Gal*p*4,6-Pyr(1→ (minor)	7
3-(4-) Gal	ND	3

[a]Small amounts of Glc and Man derivatives were detected, but not included in this table.
[b]Methylated at the positions indicated.
[c]Sulfate groups are highlighted.
[d]These units could derive from the type-II AG glycans usually found in AGPs.

dodecyl sulfate polyacrylamide gel electrophoresis (SDS–PAGE) (Figure 7A) and one major band with a high-molecular weight (∼200–250 kD) that corresponds to AGP and extensin epitopes was detected (JIM-16 and JIM-20/LM-1 mAbs, respectively). On the other hand, LM-1 showed two close bands in the same M_r range. The TB*O* staining patterns of the pAGS in A1 (Figure 7A) did not overlap with the HRGP epitopes, suggesting that HRGPs and pAGS are different cell wall components.

β-Glucosyl Yariv reagent (β-GlcYR), known to specifically bind AGP molecules in a noncovalent manner (Yariv et al. 1962), was used to precipitate the AGP molecules from *C. fragile* cell walls (Figure 2B). The β-GlcYR precipitated material (β-GlcYR-pp) that comprised ∼0.8% (w/w) was analyzed by SDS–PAGE (Figure 7B). A weak protein band with a high-molecular weight (∼200–250 kD) was detectable with Coomassie blue (CB) and colabeled with β-GlcYR; it also reacted with JIM-16 and JIM-20 mAbs (Figure 7B), suggesting the presence of both AGP and extensin epitopes in the isolated β-GlcYR-pp (Knox et al. 1991; Smallwood et al. 1994; Yates et al. 1996). In addition, a weak labeling with TB*O* (at pH = 1) was found at higher M_r (>250 kD) compared with those bands corresponding to the HRGP epitopes, indicating a possible nonspecific coprecipitation of pAGS and HRGP epitopes (Figure 7B).

The main sugars in β-GlcYR-pp were arabinose and galactose, but also low amounts of sulfate were detected (not shown) suggesting the coprecipitation of pAGS with the HRGPs, in agreement with a TB*O* band detected before in A1 (Figure 7B). Even though linkage analysis of a β-GlcYR-pp fraction showed the presence of 3- and 3,6-linked Gal*p* units together with 5- and 3,5-linked Ara*f* residues, typical of type-II AG glycans usually present in AGPs, sulfated units were also detected as in fraction A1/F1 (not shown). This confirms that pAGS coprecipitated with the AGPs in the β-GlcYR-pp fraction. In addition, the amino acid analysis of the β-GlcYR-pp showed that 21.4% of the total Pro units (7.0 mol% of the total amino acid content) were hydroxylated at C-4 giving Hyp. Moreover, a high content of other hydroxylated amino acids, such as Ser, Thr, and Tyr, was also detected (16.7 mol%, Table S3).

The in situ distribution of AGPs and extensin carbohydrate epitopes in the cell walls from *C. fragile* was followed using several probes (Table S2; Figure 7C and E). AGP epitopes were localized with β-GlcYR (Figure 7C). In the utricle tip at longitudinal and cross-section views, β-GlcYR reacts in the inner part of the cell wall, close to the plasma membrane (Figure 7C). In addition, cell wall proteins were detected by CB staining and characteristic FTIR protein absorbance bands at 1650 cm^{-1} and 1540 cm^{-1} (Pelton and McLean 2000) in the SR-FTIR map. These cell wall proteins localize in the boundaries and in the apical region of the utricle cell walls (Figure 7D). In good agreement, AGP epitopes were not only localized with MAC-207 and JIM-16 mAbs in the inner side but also in outer faces of the utricle cell walls (Figure 7E). On the other hand, extensin epitopes (JIM-11 and JIM-20) were detectable mostly in the tip of the mucron utricles, showing that the distribution of AGP and extensin glycans were only overlapped in the apical region of the utricle cells, but not in the cell wall region close to the plasma membrane.

Discussion

Cell walls in C. fragile

The global cell wall characterization showed that the diploid thallus of *C. fragile* biosynthesizes ∼31% (w/w) of (1→4)-β-D-mannans, ∼9% w/w of pyruvylated arabinogalactan sulfate (pAGS), and low amounts (<0.8%) of AGP/extensin-like epitopes, as major carbohydrate-containing macromolecules. Based on the data presented here, the utricle cell walls have a sandwich structure with two boundary zones of HRGPs, comprising AGPs and extensins epitopes, and a central layer rich in (1→4)-β-D-mannans and pAGS. The presence of fibrillar mannans and pAGS in the same region of the cell wall suggests an important degree of interaction between both macromolecular types and could be the reason why there are still considerable amounts of pAGS in residue RM2, obtained after several sequential water extractions.

The middle area of the cell wall comprises mostly linear (1→4)-β-D-mannans. After β-mannanase treatments, the cell wall integrity was severely damaged, completely disrupted in

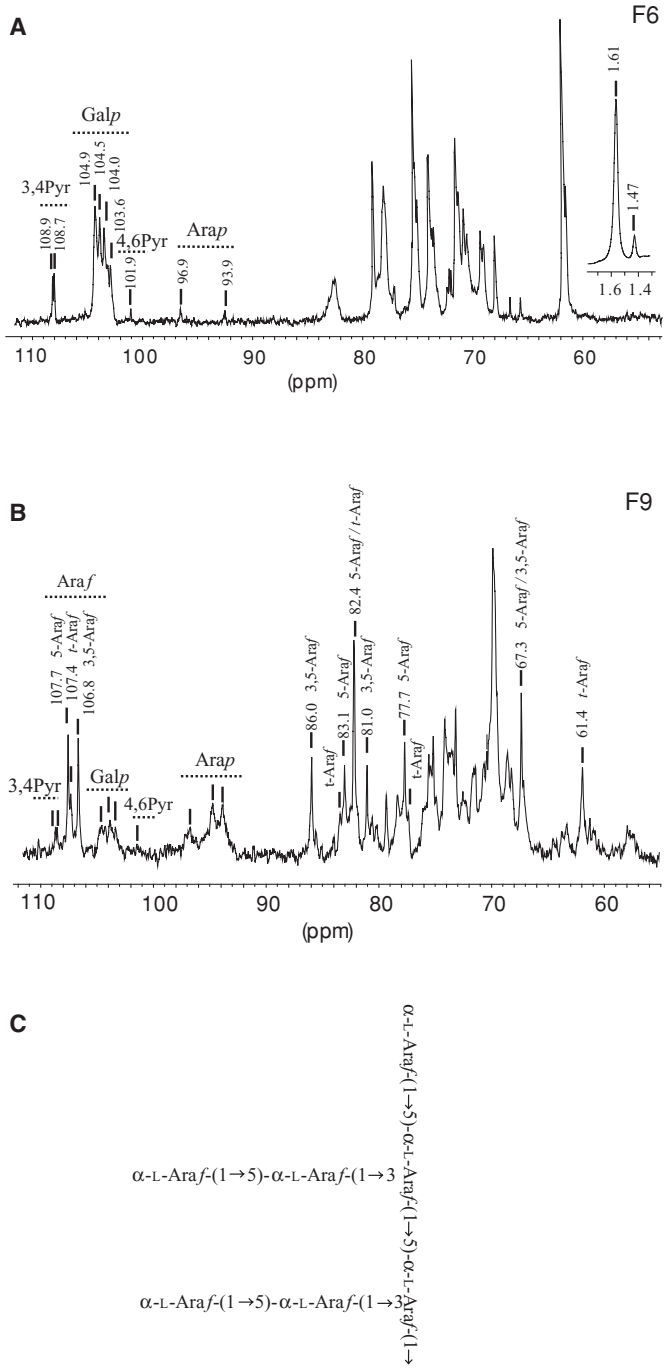

Fig. 6. Characterization of the minor fractions isolated from the pyruvylated arabingalactan sulfate fraction A1. (**A**) ^{13}C NMR spectrum of galactan-rich fraction F6. Four groups of signals corresponding to 3-(3,6)-linked β-D-Gal*p* units with different substitutions were found at 105.0–103.5 ppm together with [3,4-*O*-(1′-carboxy)-ethylidene] of pyruvic acid linked to terminal units of β-D-galactose. In addition, signals at δ_C 96.8 and 93.8 were assigned to 3-linked β-L-Ara*p*-2-(and 2,4-)sulfate and 2,3-linked β-L-Ara*p* units, respectively. Similar structural units were found by linkage analysis of this fraction (Table III). (**B**) ^{13}C NMR spectrum of arabinose-rich F9. The spectrum shows very clearly three sets of signals in the anomeric zone due to 5-linked α-L-arabinofuranosyl units, 3,5-linked α-L-arabinofuranosyl residues, and terminal α-L-arabinofuranosyl residues. In addition, the signals already described for A1/F1 that correspond to terminal 3,4-pyruvylated Gal*p* residues and 3-linked Gal*p* and Ara*p* units were also detected. (**C**) Primary structure of the furanosic arabinan present in F9, possibly as part of the type-II AG glycans typically found in AGPs. See Table IV for the NMR signal assignments.

some areas (Figure 3D), showing the important role of this polymer in cell wall assembly and stability. Two types of (1→4)-β-D-mannans have already been described for *C. fragile* cell walls: an alkali soluble-fibrillar mannan type I and an alkali-resistant fibrillar mannan type II that replaces cellulose as the main skeletal-fibrillar component (Chanzy et al. 1984), with a DP much higher than those found for other plant β-mannans (Mackie and Sellen 1969). Mannans obtained in fractions M1/M2 are possibly part of type-I mannans that would be partially soluble in hot water. In addition, in the dasycladacean *Acetabularia*, it was shown recently that the diplophase biosynthesizes also mostly noncrystalline, as well as *para*-crystalline (1→4)-β-D-mannans, with low amounts of putative substitutions on C-2, C-3, or C-6 (Dunn et al. 2007), and in *C. vermilara* low degree of substitution was detected at C-3 and C-6 (Ciancia et al. 2007). Different degree of crystallinity found in mannans would be related with the degree of substitution present in the main (1→4)-β-D-mannan backbone that clearly affects the way in which the chains are packed by H-bonding and organized into the macromolecular structure. The detection of small amounts of 4-linked 3-substituted mannosyl units (in fraction M1) indicated that a very small degree of substitution cannot be ruled out for the soluble mannans from *C. fragile* (Ciancia et al. 2007), but no substitution was found in this work in the insoluble moiety. From the biomechanical point of view, *C. fragile* is an order of magnitude weaker per cross-sectional area and more compliant than typical cellulosic red and brown macroalgae (Hale 2001). In line with these observations, it was hypothesized that the presence of low-crystalline mannans in the gametophytes of *Acetabularia* would provide higher extensibility to the cell walls in comparison with other cellulose-rich cell walls (Dunn et al. 2007). Whether these material properties are a consequence of the complete lack of cellulose and high levels of cell wall mannans or are related with a siphonous construction of the thallus, or both, is still an open question.

The presence not only of (1→4)-β-D-mannans in coencocytic *Codium* and *Acetabularia*, but also (1→3)-β-D-xylans in other phylogenetically close coencocytic seaweeds (e.g., *Caulerpa*), suggests that these organisms have found more than one way to develop cell walls based on cellulose-like polymers (Chanzy et al. 1984; Maeda et al. 1990; Lahaye et al. 2003). Recently, mannan synthases (ManS) that make (1→4)-β-D-(gluco)mannans were identified as cellulose synthase-like A genes (Csl*A*) in several vascular plants (Dhugga et al. 2004; Liepman, Wilkerson et al. 2005; Liepman, Nairn et al. 2007; Suzuki et al. 2006). Since Csl*A*s enzymatic activities and protein sequences seem to be well conserved along plant evolution (Dhugga et al. 2004; Liepman et al. 2005, 2007), it is tempting to hypothesize that some homologous genes of Csl*A* would be highly expressed in *Codium*.

Sulfated polysaccharides and the marine environment

The galactan moiety of the pAGS in *C. fragile* presents the general structural pattern of the galactan backbone typical of this genus (Bilan et al 2006; Ciancia et al. 2007; Farias et al. 2008). Sulfate groups in the pAGS from *C. fragile* were located mainly at C-4, C-6, or both positions of the 3-linked β-D-Gal*p* residues and also at C-2 and C-4 or only C-4 of the 3-linked β-L-Ara*p* units with a similar pattern of sulfate substitution to that found previously for the galactans investigated (Bilan et al. 2007) and that suggested before for the arabinan moiety

Table IV. Chemical shift assignments of the NMR spectra of the pyruvylated arabinogalactan sulfate (pAGS) fractions **A1/F1**, pyruvylated galactan sulfate (pGS) fraction **F6**, and mixed AGP and pAGS structures in **F9**

	Chemical shift (ppm)					
Type of unit	H1/C1	H2/C2	H3/C3	H4/C4	H5/C5	H6/C6
pAGS/pGS[a]						
→3) L-Ara*p***2,4S**(1→	5.38/96.8					
→3) L-Ara*p***2,4S**(1→	5.45/94.8					
→3)L-Ara*p***4S**(1→	5.41/94.4					
→2,3)L-Ara*p*(1→	5.31/93.8					
3,4Pyr-D-Gal*p*(1→3	4.75–4.65/105–103	3.55/74.2	4.27/78.7	4.19/75.5	4.04/73.3	3.86/61.6
→3)D-Gal*p***4,6S**(1→3	4.75–4.65/105–103					4.03; 3.94/70.2
→3,6)D-Gal*p***4S**(1→3	4.75–4.65/105–103	3.82/71.6	4.02/79.3	4.80/78.1	4.05/74.5	nd
→3)D-Gal*p***4S**(1→6	4.55–4.45/105–103	3.82/71.6	4.08/79.0	4.82/78.1	3.81/75.4	3.64/61.6
AGP-like						
t-L-Ara*f*(1→	5.09/107.4	82.4	77.4	84.0	61.2	
→5)L-Ara*f*(1→	5.25/107.7	82.4	77.7	83.1	67.3	
→3,5)L-Ara*f*(1→	5.25/106.7	81.1	86.0	82.4	67.3	
→3)D-Gal*p*(1→6	4.55–4.45/105–103	3.78/71.2	3.84/83.3	4.20/69.5	3.71/75.6	3.77/61.8
→3,6)D-Gal*p*(1→3	4.75–4.65/105–103	3.78/71.6	3.85/83.6	4.20/69.7	3.91/74.8	4.03; 3.94/70.2

[a]Assignment of the arabinan moiety is tentative. Sulfate groups are highlighted.

(Ciancia et al. 2007). In addition, terminal 3,4-*O*-pyruvylated β-D-galactose units, together with minor amounts of 3-linked 4,6-*O*-pyruvylated β-D-Gal*p* residues, were found in the galactan moiety of the pAGS (in *C. fragile*). Overall, the level of pyruvylation on the galactose units in *C. fragile* isolated fractions (22 and 33 mol% in A1 and F1, respectively) was similar to those values found recently for *C. isthmocladum* (30–40%) and *C. vermilara* (24%) and higher than those reported for the pyruvylated galactan from *C. yezoense* (15%) (Bilan et al. 2006; Ciancia et al. 2007; Farias et al. 2008). Based on the structural analysis carried out on A1/F1, we speculate that 3-linked Ara*p* units could form long side chains linked to C-6 of some 3-linked Gal*p* units that make the core backbone in the pAGS. Further studies are needed to confirm this linkage.

Cell walls from marine organisms like red and brown seaweeds, together with marine angiosperms (seagrasses, Alismatidae), usually have either sulfated galactose (in galactan sulfates, carrageenans, agarans) or sulfated fucose (in fucoidans) in their polysaccharides. On the other hand, these sulfate groups are missing in the polysaccharides from freshwater macroalgae and terrestrial plants (Carpita and Gibeaut 1993; Zablackis and Huang 1995; Les et al. 1997; Youngs et al. 1998; Stortz and Cerezo 2000; Ponce et al. 2003; Aquino and Landeira-Fernandez 2005; Estevez, Ciancia, et al. 2008). The fact that all these evolutionary distant organisms possess structurally related sulfated polysaccharides in their cell walls-intercellular matrices might be the result of convergent and extreme directional selection forces in their marine environments under high saline conditions (Aquino and Landeira-Fernandez 2005). Acidic polysaccharides with abundant sulfate groups in high ionic strength media such as seawater would remain strongly charged providing mechanical stress resistance, hydration by gel formation, and finally, they would act as ionic and osmotic regulators (Kloareg and Quatrano 1988). The presence of pyruvylated galactans is not exclusive of the green seaweed *Codium*, since they were found in some red seaweed groups as pyruvic acid ketals at 4,6- of the 3-linked β-D-Gal*p* units (Lahaye et al. 1989; Chiovitti, Bacic, Craik, Munro, et al. 1997, Chiovitti, Bacic, Craik, Sharon, et al. 1997). It is unknown whether these pyruvylated Gal*p* units provide any additional biological function to that of the sulfate groups in these cell walls. It must be considered, however, that pyruvylation is not a general characteristic of seaweed polysaccharides, as it is only present in some genera.

Cell wall HRGPs in Codium

Thompson and Preston (1967) first reported the existence of Hyp-containing proteins in the cell walls of green seaweeds, including *Codium*. In our work, the presence of AGPs in *C. fragile* cell walls is well supported by the amounts of Hyp detected in the cell wall fractions (Table S3), positive β-Glc-YR, and JIM-16/MAC207 labeling (Figure 7C and E). In addition, characteristic type-II AG-glycan structures were detected in A1/F1, F9 (Tables II and III), and β-GlcYR-pp fractions, indicating the presence of a galactan core composed of 3- and 3,6-linked β-D-Gal*p* units and variable levels of 5-(3,5)-linked and terminal α-L-Ara*f* units (Table IV). Based on our results in *C. fragile*, no or low degree of sulfation would occur in the HRGPs, as deduced from SDS–PAGE migration profiles of the pAGS and AGP and extensin epitopes in the β-GlcYR-pp fraction (Figure 7A and B). Moreover, the fact that many well-known monoclonal antibodies and β-GlcYR recognize AGPs and extensin epitopes (β-GlcYR only labels AGPs) in intact cell walls from *C. fragile* favors this hypothesis. Further experiments are in progress to address the diversity and the exact structure of these HRGPs in *C. fragile* cell walls.

The major *O*-glycosylated amino acid in HRGPs, Hyp, was detected in many different green algal groups with the exception of Charales (Thompson and Preston 1967; Gotelli and Cleland 1968). Additionally, two expressed sequenced tags (ESTs) from the green seawed *Ulva linza* were also associated with HRGPs (Stanley et al. 2005) and several extensins were the main extracellular matrix components in volvocacean green algae (Lamport and Miller 1971; Roberts 1974; Ender et al. 2002; Hallmann 2006). Besides, AGP and extensin epitopes were immunolocalized in the green alga *Oedogonium* (Estevez, Leonardi, et al. 2008), and AGP epitopes were mapped on the cell walls of the green algae *Micrasterias* and *Pleurotaenium* (Luetz-Meindl and Brosch Salomon 2000; Domozych

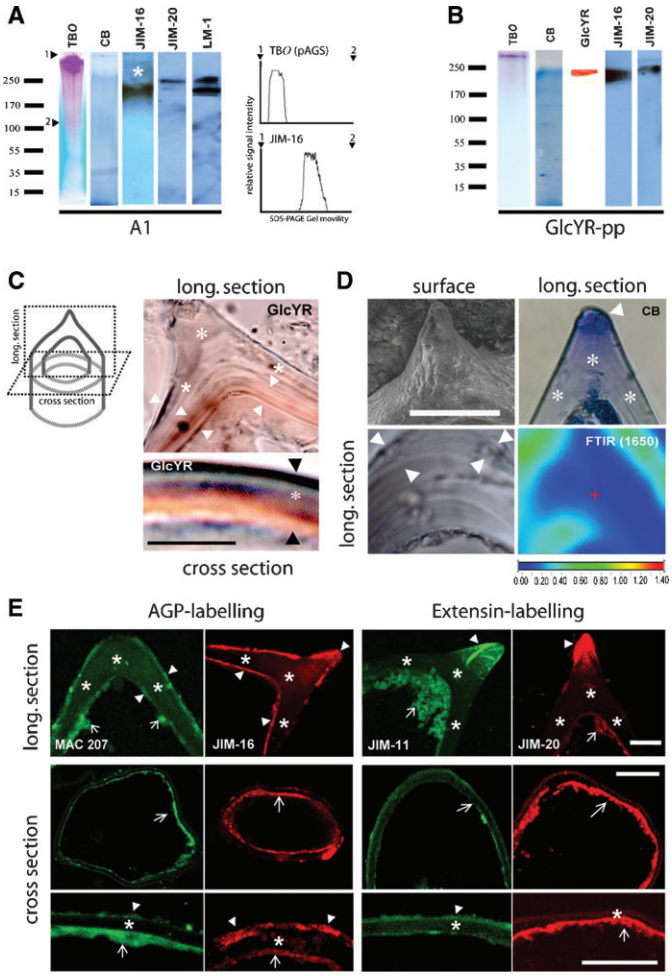

Fig. 7. Cell wall HRGP epitopes in *C. fragile*. (**A**) SDS–PAGE analysis of the water-soluble extract A1 by TB*O* staining for sulfated polysaccharides (pAGS), JIM-16 (for AGP-glycans), and JIM-20/LM-1 immunolabelings (for extensin epitopes). In addition, PAGE profiles of the pAGS and HRGP epitopes were analyzed with Image J. Loading sites of these samples are shown by an arrowhead (see *Material and methods*). No detectable overlapping was found between sulfated groups and HRGP epitopes. (**B**) β-Glucosyl Yariv precipitated material (β-GlcYR-pp) was subjected to SDS–PAGE and protein gel blotting. β-GlcYR-pp appeared as a defined band on a denaturing gel with an apparent molecular mass in the region of ∼200 kD. CB staining of an equivalent band in β-GlcYR-pp is also shown. The immunoblot indicated that the same band in the β-GlcYR-precipitated AGPs was bound by JIM-16 (AGP-glycans) and JIM-20 (extensins-glycan) antibodies. Loading per line was 10 μg carbohydrate for the β-GlcYR-pp. This suggests that the β-GlcYR-pp from *C. fragile* presents not only AGP but also extensin epitopes. (**C–D**) In situ localization of AGPs with β-glucosyl Yariv reagent (β-GlcYR) and proteins associated with HRGP epitopes in the cell wall of *C. fragile*. (**C**) Positive β-GlcYR staining indicates the presence of AGP epitopes in the utricle tip cell walls (middle) and in the utricle in cross-section (right). Scale bar = 40 μm. No reaction was detected with α-galactosyl Yariv reagent (not shown). (**D**) Utricle tip surface by ESEM, top left. Protein localization shown by CB staining (top right). Chemical images using SR-FTIR micro-spectroscopy of a longitudinal section of the cell wall area from the mucron tip. A cell wall area of 80 × 60 μm was mapped with a 10 × 10 μm window resolution (bottom left). Only the protein band at 1650 cm^{-1} is shown (bottom right). The color gradient used in the chemical image is shown below. (**E**) In situ immunolocalizacion by laser scanning confocal microscopy (LSCM) of AGP and extensin epitopes in the cell wall of *C. fragile*. Utricles in a longitudinal section view (top panels). Scale bar = 40 μm. Utricles in transverse section (lower panels). Scale bar = 40 μm. See Table S2 for antibodies specificity. In all the cases, the epitope-labeling in the cytoplasm is indicated with arrows whereas most reactive cell wall areas are indicated with arrowheads. The absence of labeling is shown with asterisks (*).

et al. 2007). Based on all these evidences, it seems that HRGPs are widespread among the diverse green algae and seaweeds, including phylogenetically distant marine and freshwater groups.

HRGPs have been proposed to be involved in many aspects of growth and development, ranging from wall architecture and assembly to cell proliferation, cell–cell recognition, and cell expansion (Seifert and Roberts 2007 and quotations therein). Although the precise roles of most individual AGPs remain unclear, biological activities have been identified in *Arabidopsis* for few AGPs, such as "xylogen," a protein with an AGP-like region that seems to be necessary for mediating local and inductive cell–cell interactions required for xylem differentiation (Motose et al. 2004). Other AGPs have been implicated in female gametogenesis (*AtAGP18*), Agrobacterium binding (*AtAGP17/RAT1*), abscisic acid (ABA) signaling during seed germination (*AtAGP30*), and cell–cell adhesion (*AtFLA4*) (Nam et al. 1999; Shi et al. 2003; van Hengel and Roberts 2003; Acosta-Garcia and Vielle-Calzada 2004; Gaspar et al. 2004). In addition, classical AGPs were suggested to act as pectin plasticizers by reducing the formation of pectate gels and enhancing cell expansion (Lamport et al. 2006). The apical high concentration of AGP epitopes in the thallus of *C. fragile* suggests a relationship with apical cell expansion in the tip growing cells, as it was clearly demonstrated for *PpAGP1* in the moss protonemal growth and for *NaTTS* in the tip growth of pollen tubes (Mollet et al. 2002; Lee et al. 2005).

On the other hand, extensins have been proposed to contribute to wall architecture, increase tensile strength, participate in cell plate formation, and contribute to defense responses by forming interpenetrating cross-linked networks in the wall, possibly through di-isodityrosine (di-IDT) and pulcherosine intermolecular cross links (Brady et al. 1998; Held et al. 2004). In particular, At*Ext3* was found to form a positive charge self-assembled scaffold essential for cell plate formation at the embryo stage, and possibly allowing an ordered deposition of the pectin matrix in the new wall (Cannon et al. 2008). Since *Codium* and all Bryopsidales are composed of continuous siphons lacking cross cell walls (and cell plate formation), it is possible that the apical extensin scaffold would provide mechanical support just after or during apical expansion. It would be interesting to test if the addition of high affinity AGP and extensin-binding molecules (e.g., β-GlcYR, JIM-16, and JIM-20 mAbs) affects the normal cell growth and development in *Codium*.

In summary, *C. fragile* represents unique cell wall architecture when compared with other seaweeds and vascular plants cell walls, given by the presence of mannans, pAGS, and HRGP epitopes, as major carbohydrate-containing polymers. This study is the first direct evidence that shows the presence of AGP-like structures and extensin epitopes in a seaweed cell wall. A detailed knowledge of how this mannan-rich cell walls are made and assembled in *Codium* cells (and in other siphonous seaweeds) including their similarities and differences from those in green algae and land plant groups would provide insights into this alternative cell wall architecture outside the cellulose scaffold.

Material and methods

Algal sample

Samples of *C. fragile var. novae zelandiae* (Suringar) Hariot were collected in Puerto Deseado (Santa Cruz, Argentina) and

identified according to Boraso and Piriz de Nuñez de la Rosa (1975). The voucher material of *C. fragile* was deposited in the herbarium of the Museo Bernardino Rivadavia Buenos Aires, Argentina (B.A. 40464). Algal material was composed only of sterile diplophase thalli, since no gametangia structures were observed.

In situ immunolocalization

The algal material was fixed in 4% formaldehyde, dehydrated in EtOH series, and embedded in paraplast (Fisher). Cross-sections of 10 μm were collected on ProbeOn microscope slides (Fisher), and after the removal of the resin with histoclear, they were blocked in PBS containing 5% (w/v) fat-free milk powder (5% MPBS) for 30 min. Rat monoclonal antibodies specific for carbohydrate epitopes (see Table S2 for specificity) were used: arabinosides of the extensin type (JIM-11 and JIM-20) and AGP glycan (JIM-16 and MAC 207) in 5% MPBS. The primary antibody (dilution 1:50–1:1000) was incubated for 1 h at RT and washed with PBS (2×). For visualizing the antibody binding, a secondary antibody anti-rat-IgG coupled with Alexa Fluor 488 (Molecular Probes) (1:1000) in 5% MPBS was added for 1 h at RT. After washing with PBS for 5 min (2×), the samples were observed in a Laser Scanning Confocal Microscope (see below). In order to localize the (1→4)-β-D-Man*p* units, a specific anti-mannan rabbit antibody (Mab) developed by Handford et al. (2003) was used (dilution 1:100). As a secondary antibody, an anti-rabbit-IgG coupled with Alexa Fluor 565 (Molecular Probes) (dilution 1:250) was used. Primary antibodies were omitted in all cases for labeling procedure that acted as a control.

Laser scanning confocal imaging and environmental scanning electron microscopy

Confocal imaging was performed using an MRC 1024 laser scanning confocal head (Bio-Rad, Hercules, CA) mounted on a Diaphot 200 inverted microscope (Nikon, Tokyo, Japan), a Zeiss 510 laser scanning confocal microscope, and a Leica TCS SP2 AOBS. The samples were excited with two lasers (Ar/Kr and He/Cd) at 488 nm and 522/520 nm for Alexa Fluor. Samples were mounted on cover slips in glycerol:water (1:1). All images were processed with Adobe Photoshop 7.0 (Adobe Systems, Mountain View, CA). For ESEM, the material already fixed in formaldehyde was observed under low vacuum conditions at 60.0 Pa, 12.5 kV, with a gaseous SED detector in a Quanta 200 (FEI, OR).

Light microscopy and histochemistry

For light microscopy (LM), semithin sections (∼5–7 μm) were mounted on glass slides, and then observed with a Carl Zeiss Axiolab microscope (Carl Zeiss, Jena, Germany). The staining procedures used in LM histochemical characterization based on Krishnamurthy (1999) were carried out on fixed tissues and included (i) TB*O* (0.05% w/v) in 0.1 M HCl at pH 1.0 that stains sulfated polysaccharides (red-purple, γ metachromasia); (ii) RR (0.0001%) in aqueous solution for acidic polysaccharides (red); (iii) CB; (iv) CW (0.1% w/v) in the aqueous solution for (1→3), (1→4)-β-, and (1→4)-β-glucans (Wood et al. 1983); (v) β-glucosyl Yariv phenyl glycoside (β-GlcYR; 1,3,5-tris-[4-β-D-glucopyranosyl-oxyphenylazo]-2,4,6-trihydroxybenzene) was used for localized total AGPs due to its specificity and α-galactosyl Yariv phenyl glycoside (α-GalYR; 1,3,5-tris-[4-α-D-galactopyranosyl-oxyphenylazo]-2,4,6-trihydroxybenzene) was used as a control (Yariv et al. 1962). Cross- and longitudinal sections of the thallus were incubated overnight at 4°C in 1% in NaCl (w/v, two times) Yariv solutions.

Extraction of the polysaccharides

The extraction procedure was described elsewhere (Ciancia et al. 2007). Briefly, the milled plants (100 g) were extracted twice with EtOH (1 L) for 3 h at RT. The residue from the alcohol extraction was extracted with H_2O (20 g/L) at room temperature for 18 h giving a product, which was recovered from the supernatant by dialysis and freeze-dried (fraction A1). The residue from the first H_2O extraction was extracted one more time under similar conditions to give fraction A2. The residue from the RT H_2O extraction was extracted twice for 3 h with H_2O at 90°C, giving the soluble fractions M1 and M2, and the residue RM2.

Carbohydrate immuno dot-blot assay

Five microliters of the water-diluted cell wall extracts and residue RM2 at three different concentrations, 4, 2, and 1 μg/μL, were applied into nitrocellulose membranes. After drying the membrane for 30 min, blots were blocked with 5% MPBS for 1–2 h. The primary antibody was used in the variable concentration (1:50–1:1000) in 5% MPBS during 3 h. After washing with TTBS (Tween 0.05% [v/v] in 1× PBS) twice and one with 1× PBS, blots were incubated under the secondary antibody anti-rat IgG coupled to alkaline phosphatase for 1 h. After washing as described before, the blots were developed in 5-bromo-4-chloro-3-indolyl phosphate and nitroblue tetrazolium for less than 10 min at RT until color reaction was observed. The experiment was repeated three times. See Table S2 for antibodies specificity.

Purification of AGPs

To extract AGPs, 900 mg (dry weight) of freeze-dried seaweed was ground to a fine powder in liquid nitrogen. Ground tissue was added to 5 mL of extraction buffer (50 mM Tris–HCl, pH 8.0, 10 mM EDTA, 0.1% β-mercaptoethanol, and 1% (w/v) Triton X-100) and incubated at 48°C for 3 h. Samples were centrifuged for 10 min at 14,000 × *g*. The supernatant was precipitated with 5 volumes of ethanol (at 4°C, overnight). The pellet was resuspended by vortex mixing in 5 mL of 50 mM Tris–HCl, pH 8.0. The insoluble material was removed by centrifugation, and the supernatant was retained. The pellet was resuspended in an additional 5 mL of 50 mM Tris–HCl, pH 8.0, and the soluble material (after centrifugation) was pooled with the first supernatant. The buffer-soluble material was freeze-dried overnight to concentrate the sample. The dried samples were resuspended in 250–500 μL of 1% (w/v) NaCl and transferred to 2 mL microcentrifuge tubes. AGPs were precipitated with the GlcYR as described in Gane et al. (1995). As a control, α-galactosyl Yariv reagent was used instead of the β-GlcYR and no precipitate material was obtained.

Electrophoresis and Western-blot analysis

Agarose gel electrophoresis was performed in a 1% (w/v) gel poured in a 1× TBE buffer (0.045 M Tris-borate, 0.001 M

EDTA). —Twenty to eighty micrograms of each sample was loaded in the gel and constant current (40 mV) was applied for 60 min. The gel was visualized with 1% (w/v) TB*O* (pH = 1.0) for sulfated polysaccharides. For Western blot analysis, 200–300 μg of sample was solubilized in 50 μL of 2× Laemmli buffer (125 mM Tris–Cl, pH. 6.8, 4% (w/v) SDS, 20% (v/v) glycerol, 2% (v/v) β-mercaptoethanol, 0.001% (w/v) bromophenol blue) containing 10 μL protease inhibitor cocktail (Sigma, St. Louis, MO) and immediately transferred to ice. The samples were boiled for 5 min and 15–20 μL and loaded on 4–20% SDS–PAGE. In all the cases, the glycoproteins/proteoglycans were separated by electrophoresis and transferred to nitrocellulose membranes. Rat IgG antibodies for AGPs (JIM-16 and MAC207) and extensins (JIM-20 and LM-1) recognition were used at dilutions of 1:500–2000 and visualized by incubation with anti-rat IgG secondary antibodies conjugated to horseradish peroxidase (1:1000) followed by a chemiluminescence reaction (Super-Signal; Pierce Chemical, Rockford, IL). See Table S2 for antibodies specificity. In addition, the same samples were loaded into 4–20% SDS–PAGE and run under the same conditions as described before. Sulfated polysaccharides were visualized with 1% (w/v) TB*O* (pH = 1.0). Migration patterns of pAGS and AGP-glycans in the SDS–PAGE and nitrocellulose membranes were analyzed using Image J 1.34 software and the images were processed with Adobe Photoshop 7.0 (Adobe Systems, Mountain View, CA).

Chemical analyses

Chemical analyses were performed as described in Ciancia et al. (2007). In addition, the total carbohydrate content of RM2 was analyzed by a phenol–sulfuric acid method adapted for insoluble material (Ahmed and Labavitch 1977). To determine the monosaccharide composition of RM2, the sample (1–3 mg) was dissolved in 100% TFA (37°C, 1 h), followed by dilution of the acid to 80%, heating at 100°C for 1 h, and further dilution to 2 M to achieve the regular hydrolysis conditions, reduction with $NaBH_4$ and acetylation (Morrison 1988). For these residues, total nitrogen and sulfur were estimated, after total degradation of the sample, by conversion to N_2 and SO_2, respectively. The mixtures of gases were separated by gas chromatrography with a porapac column in Carbo Erba EA 1108 chromatograph (Milan, Italy), using a thermic detector; the total protein content was expressed using a factor of 5.13. For methylation analyses, samples (5–10 mg) were converted into the corresponding triethylammonium salt and methylated according to Ciucanu and Kerek (1984). Desulfation was carried out by the microwave-assisted method described by Navarro et al. (2007); desulfated products DsA1, DsF1, and DsF6 were obtained in high yields (55–70%). 20.6, 12.2, 19.4% of initial sulfate contents in A1, F1, and F6 were lowered to 3–4% in DsA1, DsF1, and DsF6. An aliquot of the desulfated products was methylated as described in Ciucanu and Kerek (1984), without previous isolation of the product. Amino acid composition of the samples was determined at the Michigan State University macromolecular facility (East Lansing, MI).

Ion-exchange chromatography

A1 was chromatographed on DEAE-Sephadex A-25. The sample (1 g) was dissolved in water and applied to a column (90 × 1.5 i.d.), previously stabilized in H2O. The first elution solvent was water and then NaCl solutions of increasing concentration up to 4 M. Fractions of 7 mL were collected. Finally, the phase was boiled in a 4 M NaCl solution. The presence of carbohydrates in the samples was detected by the phenol sulfuric acid method (Dubois et al. 1956); after obtaining blank readings, the eluant was replaced by another with higher concentration of NaCl. The products obtained were dialyzed (MWCO 3500) and freeze-dried. Analytical IEC of F1 (20 mg) was carried out as described before in a column of 16 × 1 cm i.d. and fractions of 2 mL were collected.

FT-IR and SR-FT-IR microspectroscopy

Fourier-transform infrared spectra were recorded from 4000 to 250 cm^{-1} with a 510P Nicolet FT-IR spectrophotometer (Madison WI), using films prepared by drying aqueous solutions of the extracts and KBr discs for RM2. Sixty-four scans were taken with a resolution of 2–4 cm^{-1}. For SR-FTIR microspectroscopy, thin sections (∼10 μm) of *Codium* thallus were obtained. Cross-sections were transferred to low e-microscope slides (MirrIR, Kevley Tech, Chesterland, OH) and FT-IR reflection spectra were acquired at the infrared spectro-microscopy beamline 1.4.3 at the Advance Light Source (ALS, Berkeley, CA). The synchrotron light was used as an external source for a Nicolet 760 FTIR bench (Madison WI). The beamline only allows light between 10,000 and 400 cm^{-1} to continue onto the sample with diffraction-limited spot (3–10 μm diameter) with high brightness (1.3×10^{-2} mW μm^{-2}). For chemical imaging, 48–96 spectra were recorded over the region 4000 to 650 cm^{-1} with a spectral resolution of 4 cm^{-1} and 64 scans coadded for Fourier transform processing to produce one spectrum. A background spectroscopic image file was collected from an area free of sample. Scanned visible images were obtained using a charge-couple device (CCD) camera linked to the infrared images. Stage control, data collection, and processing were performed on the OMNIC 7.2 (Thermo-Nicolet, Madison, WI) together with Win-Das software (Wiley, NY). At least 10 sections were analyzed. To reveal the major spectral differences in the cell wall area, a mathematical operation of data compression called principal component analysis (PCA) by a covariance matrix method (Kelmsley 1998) was applied to all the spectra. The variability in each individual spectrum relative to the mean for the population is then represented as a smaller set of values (axes) termed principal components (PCs).

NMR spectroscopy

A1, F1, and RM2dig were analyzed by one- and two-dimensional NMR experiments (HSQC and HMBC) carried out with a Varian Unity INOVA 600 MHz (Palo Alto, CA) spectrometer operating at ^1H and ^{13}C frequencies of 600 and 150 MHz, respectively. Pulse sequences for 2D techniques were supplied by the spectrometer manufacturers. Data were processed with Sparkly 3.113 and NUTS NMR 2D version. 500 MHz ^1H NMR and proton decoupled the 125 MHz ^{13}C NMR spectra of F6, and F9 were recorded on a Bruker AM500 (Hanau, Germany) at RT, with external reference of TMS. Samples were exchanged in 99.9% D_2O (0.5 mL) four times. Chemical shifts were referenced to internal acetone (δ_C 31.1) or methanol (δ_C 50.15).

Enzymatic treatments

The β-mannanase treatment was performed with an endo-(1→4)-β-D-mannanase (AN3358.2; Bauer et al. 2006) on the enriched mannan fraction RM2 (850 mg) in 50 mM acetate buffer, pH 5.5, at 37°C overnight and repeated three times. The supernatant was filtered with a Centricon centrifugation device (MWCO 5000 kDa), and then freeze-dried. The oligosaccharides obtained were desalted in a PD-10 column (170 mg) and the remaining residue was weighted (RM2dig, 350 mg). The β-mannanase treatment was also performed in situ over semithin cross-sections obtained from *C. fragile* after the removal of paraplast resin. The cross-sections ($n = 40$) were incubated with the same endo-(1→4)-β-D-mannanase described above. A buffer without the enzyme was used as a negative control. The supernatant of both treatments was collected and the monosaccharide analysis was performed as described in Ciancia et al. 2007. Cross-section area was measured using Image J 1.34 software.

Analysis of mannose-containing oligosaccharides by PACE

Commercial ivory nut (1→4)-β-D-mannan (∼4 mol% Gal), gum-guar galactomannan (∼28 mol% Gal), and konjac glucomannan (∼40 mol% Glc) were used as standards. RM2dig from *C. fragile* and the commercial polysaccharides were prepared according to Goubet et al. (2002) and Handford et al. (2003), except that they were treated with aqueous ammonia (200 μL) for 2 h before drying in a Speedvac (ThermoLife Science, Hampshire, UK). RM2dig and the standards (2 mg) were digested with Man5A (5.0 μg) from Cellvibrio japonicus in 0.1 M ammonium acetate at pH 6.0 overnight and 0.1 mg mL^{-1} BSA in a total volume of 2 mL.

Supplementary Data

Supplementary data for this article is available online at http://glycob.oxfordjournals.org.

Funding

University of Buenos Aires (UBACyT X016); the National Research Council of Argentina, CONICET (Res. No. 674/04 and PIP 5699); a U.S. DOE (grant to C. Sommerville, Carnagie Institution for Science, Stanford, CA) and AGENCIA (PICT 2006-00983) to J.M.E; and BBSRC (PACE experiments to P.D.).

Acknowledgements

The authors gratefully acknowledge A. S. Cerezo for the critical reading of the manuscript and C. Somerville for providing most of the antibodies used in this study and also making available to J.M.E. the infrastructure of Carnegie Institution of Washington (Stanford University). Without his support, this work would have not been possible. The authors also thank the assistance of X.L. Yu for the PACE experiments, M.C. Martin (ALS, Berkeley, CA), and T.K. Raab with the SR-FTIR microspectroscopy analysis (ALS, Berkeley, CA) and CG-MS, and finally, S. Lynch for the NMR experiment (NMR Facility, Stanford University). The Advanced Light Source is supported by the Director, Office of Science, Office of Basic Energy Sciences, the U.S. Department of Energy under Contract No. DE-AC02-05CH11231.

Conflict of interest statement

None declared.

Abbreviations

AGPs, arabinogalactan proteins; CB, coomasie blue; CW, calcofluor white; ESEM, environmental scanning electron microscopy; β-GlcYR, β-glucosyl Yariv reagent; HRGPs, hydroxyproline rich-glycoproteins; IDA, immuno dot-blot assay; IEC, ion-exchange chromatography; LSCM, laser scanning confocal microscopy; mAb, monoclonal antibody; pAGS, pyruvylated arabinogalactan sulfate; PACE, polysaccharide analysis by carbohydrate gel electrophoresis; PCA, principal component analysis; RR, ruthenium red; SDS–PAGE, sodium dodecyl sulfate polyacrylamide gel electrophoresis; SR-FTIR microspectroscopy, synchrotron radiation Fourier transform infrared couple to a microscope; TB*O*, toluidine blue ortochromatic; TFA, trifluoroacetic acid; TMS, tetramethylsilane.

References

Acosta-Garcia G, Vielle-Calzada JP. 2004. A classical arabinogalactan protein is essential for the initiation of female gametogenesis in *Arabidopsis*. *Plant Cell*. 16:2614–2628.

Ahmed AER, Labavitch JM. 1977. A simplified method for accurate determination of cell wall uronide content. *J Food Biochem*. 1:361–365.

Aquino RS, Landeira-Fernandez AM. 2005. Occurrence of sulfated galactans in marine angiosperms: Evolutionary implications. *Glycobiol*. 15:11–20.

Bauer S, Vasu P, Persson S, Mort AJ, Somerville CR. 2006. Development and application of a suite of polysaccharide-degrading enzymes for analyzing plant cell walls. *Proc Natl Acad Sci USA*. 103:11417–11422.

Bilan MI, Vinogradova EV, Shashkov AS, Usov AI. 2006. Isolation and preliminary characterization of a highly pyruvylated galactan from *Codium yezoense* (Bryopsidales, Chlorophyta). *Bot Mar*. 49:259–262.

Bilan MI, Vinogradova EV, Shashkov AS, Usov AI. 2007. Structure of a highly pyruvylated galactan sulfate from the pacific green alga *Codium yezoense* (Bryopsidales, Chlorophyta). *Carbohydr Res*. 342:586–596.

Bock K, Pedersen C, Pedersen H. 1986. Carbon-13 nuclear magnetic resonance data for oligosaccharides. *Adv Carbohydr Chem Biochem*. 42:193–225.

Boraso AL, Piriz de Nuñez de la Rosa ML. 1975. Especies del género *Codium* (Chlorophyta) en la Costa Argentina. *Physis Secc A*. 34:245–256.

Brady JD, Sadler IH, Fry SC. 1998. Pulcherosine, an oxidative coupled trimer of tyrosine in plant cell walls: Its role in cross-link formation. *Phytochem*. 47:349–353.

Cannon MC, Terneus KA, Hall Q, Tan L, Wang Y, Wegenhart B, Chen L, Lamport DTA, Chen Y, Kieliszewksi MJ. 2008. Self-assembly of the plant cell wall requires an extensin scaffold. *Proc Natl Acad Sci USA*. 105:2226–2231.

Carpita NC, Defernez M, Findlay K, Wells B, Shoue DA, Catchpole G, Wilson RH, McCann MC. 2001. Cell wall architecture of the elongating maize coleoptile. *Plant Physiol*. 127:551–565.

Carpita NC, Gibeaut DM. 1993. Structural models of primary cell walls in flowering plants: Consistency of molecular structure with the physical properties of the walls during growth. *Plant J*. 3:1–30.

Chanzy HD, Grosrenaud A, Vuong R, Mackie W. 1984. The crystalline polymorphism of mannans in plant cell walls and after recrystallisation. *Planta*. 161:320–329.

Chiovitti A, Bacic A, Craik DJ, Munro SLA, Kraft GT, Liao ML. 1997. Cell-wall polysaccharides from Austalian red algae of the family *Solieriaceae* (Gigartinales, Rhodophyta): Novel, highly pyruvated carrageenans from the genus *Callophycus*. *Carbohydr Res*. 299:229–243.

Chiovitti A, Bacic A, Craik DJ, Sharon L, Munro SLA, Kraft GT, Liao ML. 1997. Carrageenans with complex substitution patterns from red algae of the genus *Erythroclonium*. *Carbohydr Res*. 305:243–252.

Ciancia M, Quintana I, Vizcargüénaga MI, Kasulin L, Dios A, Estevez JM, Cerezo AS. 2007. Polysaccharides from the green seaweeds *Codium fragile* and *C. vermilara* with controversial effects on hemostasis. *Int J Biol Macromol*. 41:641–649.

Ciucanu I, Kerek K. 1984. A simple and rapid method for the permethylation of carbohydrates. *Carbohydr Res*. 134:209–217.

Davis AL, Hoffmann RA, Russell AL, Debet M. 1995. ^{1}H- and ^{13}C-NMR characterization of the digalactosylmannopentaose liberated from legume seed galactomannan by b-mannanase action. *Carbohydr Res.* 271:43–54.

Dhugga KS, Barreiro R, Whitten B, Stecca K, Hazebroek J, Randhawa GS, Dolan M, Kinney AJ, Tomes D, Nichols S, et al. 2004. Guar seed beta-mannan synthase is a member of the cellulose synthase super gene family. *Science*. 303:363–366.

Domozych DS, Elliott L, Kiemle SN, Gretz MR. 2007. *Pleurotaenium trabecula*, a desmid of wetland biofilms: The extracellular matrix and adhesion mechanisms. *J Phycol*. 43:1022–1038.

Dourado F, Cardoso SM, Silva AMS, Gama FM, Coimbra MA. 2006. NMR structural elucidation of the arabinan from *Prunas dulcis* immunological active pectic polysaccharides. *Carbohydr Pol*. 66:27–33.

Dubois M, Gilles KA, Hamilton JK, Rebers PA, Smith F. 1956. Colorimetric method of determination of sugars and related substances. *Anal Chem*. 28:350–356.

Dunn EK, Shoue DA, Huang X, Kline RE, MacKay AL, Carpita NC, Taylor IEP, Mandoli DF. 2007. Spectroscopic and biochemical analysis of regions of the cell wall of the unicellular "mannan weed", *Acetabularia acetabulum*. *Plant Cell Physiol*. 48:122–133.

Ender F, Godl K, Wenzl S, Sumper M. 2002. Evidence for autocatalytic cross-linking of hydroxyproline-rich glycoproteins during extracellular matrix assembly in *Volvox*. *Plant Cell*. 14:1147–1160.

Estevez JM, Ciancia M, Cerezo A. 2008. The system of sulfated galactans from the red seaweed *Gymnogongrus torulosus* (Phyllophoraceae, Rhodophyta). Location and structural analysis. *Carbohydr Pol*. 73:594–605.

Estevez JM, Ciancia M, Cerezo AS. 2004. The system of galactans of the red seaweed, *Kappaphycus alvarezii*, with emphasis on its minor constituents. *Carbohydr Res*. 339:2575–2592.

Estevez JM, Kiesliszewski MJ, Khitrov N, Somerville C. 2006. Characterization of synthetic hydroxyproline-rich proteoglycans with AGP- and extensin-motifs in *Arabidopsis*. *Plant Physiol*. 142:458–470.

Estevez JM, Leonardi P, Alberghina J. 2008. Cell wall carbohydrate-epitopes in the green algae *Oedogonium bharuchae f. minor* (Oedogoniales, Chlorophyta). *J Phycol*. 44(5):1257–1268.

Farias EHC, Pomin VH, Valente AP, Nader HB, Rocha HAO, Mourao PAS. 2008. A preponderantly 4-sulfated, 3-linked galactan from the green alga *Codium isthmocladum*. *Glycobiol*. 18:250–259.

Gane A M, Craik D, Munro SLA, Howlett GJ, Clarke AE, Bacic A. 1995. Structural analysis of the carbohydrate moiety of arabinogalactan-proteins from stigmas and styles of *Nicotiana alata*. *Carbohydr Res*. 277:67–85.

Gaspar Y, Johnson KL, McKenna JA, Bacic A, Schultz CJ. 2001. The complex structures of arabinogalactan proteins and the journey towards understanding function. *Plant Mol Biol*. 47:161–176.

Gaspar YM, Nam J, Schultz CJ, Lee L-Y, Gilson PR, Gelvin SB, Bacic A. 2004. Characterization of the Arabidopsis lysin rich arabinogalactan protein AtAGP17 mutant (rat1) that results in a decreased efficiency of Agrobacterium transformation. *Plant Physiol*. 135:2162–2171.

Gotelli IB, Cleland R. 1968. Differences in the occurrence and distribution of hydroxyproline-proteins among the algae. *Am J Bot*. 55:907–914.

Goubet F, Jackson P, Deery MJ, Dupree P. 2002. Polysaccharide analysis using carbohydrate gel electrophoresis: A method to study plant cell wall polysaccharides and polysaccharide hydrolases. *Anal Biochem*. 300:53–64.

Hale B. 2001. Macroalgal materials: Foiling fracture and fatigue from fluid forces. *Biological Sciences*. Stanford, CA: Stanford University Press. p. 381.

Hallmann A. 2006. The pherophorins: Common, versatile building blocks in the evolution of extracellular matrix architecture in volvocales. *Plant J*. 45(2):292–307.

Handford MG, Baldwin TC, Goubet F, Prime TA, Miles J, Yu X, Dupree P. 2003. Localization and characterization of cell wall mannan polysaccharides in *Arabidopsis thaliana*. *Planta*. 218:27–36.

Held M, Tan L, Kamyab A, Hare M, Shpak E, Kieliszewski MJ. 2004. Di-Isodityrosine is the intermolecular cross-link of isodityrosine-rich extensins analogs cross-linked in vitro. *J Biol Chem*. 279:55474–55482.

Kelmsley EK. 1998. *Discriminant Analysis of Spectroscopic Data*. Chichester, UK: Wiley.

Kieliszewski M, de Zacks R, Leykam JF, Lamport DTA. 1992. A repetitive proline-rich protein from the gymnosperm Douglas fir is a hydroxyproline-rich glycoprotein. *Plant Physiol*. 98:919–926.

Kieliszewski MJ. 2001. The latest hype on Hyp-*O*-glycosylation codes. *Phytochem*. 57:319–323.

Kieliszewski MJ, O'Neill M, Leykam J, Orlando R. 1995. Tandem mass spectrometry and structural elucidation of glycopeptides from a hydroxyproline-rich plant cell wall glycoprotein indicate that contiguous hydroxyproline residues are the major sites of hydroxyproline-*O*-arabinosylation. *J Biol Chem*. 270:2541–2549.

Kloareg B, Quatrano RS. 1988. Structure of the cell wall of marine algae and ecophysiological functions of the matrix polysaccharides. *Oceanogr Mar Biot Annu Rev*. 26:259–315.

Knox JP, Linstead PJ, Peart J, Cooper C, Roberts K. 1991. Developmentally regulated epitopes of cell surface arabinogalactan-proteins and their relation to root tissue pattern formation. *Plant J*. 1:317–326.

Krishnamurthy KV. 1999. Transmission electron microscopic cytochemistry. In: Krishnamurthy KV, editor. *Methods in Cell Wall Cytochemistry*. Boca Raton, FL: CRC Press. p. 177–226.

Lahaye M, Rondeau-Mouro C, Deniaud E, Buleon A. 2003. Solid-state 13C NMR spectroscopy studies of xylans in the cell wall of *Palmaria palmata* (L. Kuntze, Rhodophyta). *Carbohydr Res*. 338:1559–1569.

Lahaye M, Yaphe W, Viet MTP, Rochas C. 1989. ^{13}C-NMR spectroscopic investigation of methylated and charged agarose oligosaccharides and polysaccharides. *Carbohydr Res*. 190:249–265.

Lamport DTA. 1965. Hydroxyproline-*O*-glycosidic linkage of the primary cell wall extensin. *Nature*. 216:1322–1324.

Lamport DTA, Kieliszewksi MJ, Showalter AM. 2006. Salt-stress upregulates periplasmic arabinogalactan-proteins: Using salt-stress to analyse AGP function. *New Phytol*. 169:479–492.

Lamport DTA, Miller DH. 1971. Hydroxyproline arabinosides in the plant kingdom. *Plant Physiology*. 48:454–445.

Lee KJD, Sakata Y, Mau SL, Pettolino F, Bacic A, Quatrano RS, Knight CD, Knox P. 2005. Arabinogalactan proteins are required for apical cell extension in the moss *Physcomitrella patens*. *Plant Cell*. 17:3051–3065.

Les DH, Cleland MA, Waycott M. 1997. Phylogenetic studies in alismatidae: II. Evolution of marine angiosperms (seagrasses) and hydrophily. *System Bot*. 22:443–463.

Liepman AH, Nairn CJ, Willats WGT, Sørensen I, Roberts AW, Keegstra K. 2007. Functional genomic analysis supports conservation of function among cellulose synthase-like A gene family members and suggests diverse roles of mannans in plants. *Plant Physiol*. 143:1881–1893.

Liepman AH, Wilkerson CG, Keegstra K. 2005. Expression of cellulose synthase-like (Csl) genes in insect cells reveals that CslA family members encode mannan synthases. *Proc Natl Acad Sci USA*. 102:2221–2226.

Love J, Percival E. 1964. The polysaccharides of the green seaweed *Codium fragile*: Part II. The water-soluble sulphated polysaccharides. *J Chem Soc*. 3338–3345.

Luetz-Meindl U, Brosch-Salomon S. 2000. Cell wall secretion in the green alga *Micrasterias*. *J Microsc*. 198:208–217.

Mackie W, Sellen DB. 1969. The degree of polymerization and polydispersity of mannan form the cell wall of the green seaweed *Codium fragile*. *Polymer*. 10:621–632.

Maeda M, Fukushi-Fujikura Y, Otsuru O. 1990. Cellulose in the cell wall of the siphonous green alga, *Bryopsis maxima*. *Carbohydr Res*. 201:91–99.

Matsubara K, Matsuura Y, Bacic A, Liao M-L, Hori K, Miyazawa K. 2001. Anticoagulant properties of a sulfated galactan preparation from a marine green alga, *Codium cylindricum*. *Int J Biol Macromol*. 28:395–399.

Matsubara K, Matsuura Y, Hori K, Miyasawa K. 2000. An anticoagulant proteoglycan from the marine green alga, *Codium pugniformis*. *J Appl Phycol*. 12:9–14.

McCartney L, Blake AW, Flint J, Bolam DN, Boraston AB, Gilbert HJ, Knox P. 2006. Differential recognition of plant cell walls by microbial xylan-specific carbohydrate-binding modules. *Proc Natl Acad Sci USA*. 103:4765–4770.

Moller I, Sørensen I, Bernal AJ, Blaukopf C, Lee K, Obro J, Pettolino F, Roberts A, Mikkelsen JD, Knox JP, et al. 2007. High-throughput mapping of cell-wall polymers within and between plants using novel microarrays. *Plant J*. 50:1118–1128.

Mollet J-C, Kim S, Jauh G-Y, Lord EM. 2002. Arabinogalactan proteins, pollen tube growth, and reversible effects of Yariv phenylglycoside. *Protoplasma*. 219:89–98.

Morrison IM. 1988. Hydrolysis of plant cell walls with trifluoroacetic acid. *Phytochem*. 27:1097–1100.

Motose H, Sugiyama M, Fukuda H. 2004. A proteoglycan mediates inductive interaction during plant vascular development. *Nature*. 429:873–878.

Nam J, Mysore KS, Zheng C, Knue MK, Matthysse AG, Gelvin SB. 1999. Identification of T-DNA tagged *Arabidopsis* mutants that are resistant to transformation by Agrobacterium. *Molec Gen Genet*. 261:429–438.

Navarro DA, Cerezo AS, Stortz CA. 2002. NMR spectroscopy and chemical studies of an arabinan-rich system from the endosperm of the seed of *Gleditsia triacanthos*. *Carbohydr Res*. 337:255–263.

Navarro DA, Flores ML, Stortz CA. 2007. Microwave-assisted desulfation of sulfated polysaccharides. *Carbohydr Pol.* 69:742–747.

Nothnagel E. 1997. Proteoglycans and related components in plant cells. *Int Rev Cytol*. 174:195–291.

Pelton JT, McLean LR. 2000. Spectroscopic methods for analysis of protein secondary structure. *Anal Biochem*. 277:167–176.

Pennell RI, Knox JP, Scofield GN, Selvendran RR, Roberts K. 1989. A family of abundant plasma membrane-associated glycoproteins related to the arabinogalactan proteins is unique to flowering plants. *J Cell Biol*. 108:1967–1977.

Percival E, McDowell RH. 1981. Algal walls. Composition and biosynthesis. In: Tanner W, Loewus FA, editors. *Encyclopedia of Plant Physiology*, vol. 13B. Berlin: Springer. p. 277–316.

Ponce NM, Pujol CA, Damonte EB, Flores ML, Stortz CA. 2003. Fucoidans from the brown seaweed *Adenocystis utricularis*: Extraction methods, antiviral activity and structural studies. *Carbohydr Res*. 338:153–165.

Prado Fernandez J, Rodríguez Vazquez JA, Tojo E, Andrade JM. 2003. Quantitation of κ-, ι, and λ-carrageenan by mid-infrared spectroscopy and PLS regression. *Anal Chim Acta*. 480:23–37.

Roberts K. 1974. Crystalline glycoproteins cell walls of algae: Their structure, composition and assembly. *Phil Trans R Soc Lond B*. 268:129–146.

Seifert GJ, Robert K. 2007. The biology of arabinogalactan proteins. *Ann Rev Plant Biol*. 58:137–161.

Shi H, Kim Y, Guo Y, Stevenson B, Zhu JK. 2003. The *Arabidopsis* SOS5 locus encodes a putative cell surface protein and is required for normal cell expansion. *Plant Cell*. 15:19–32.

Showalter AM. 2001. Arabinogalactan-proteins: Structure, expression and function. *Cell Mol Life Sci*. 58:1399–1417.

Shpak E, Barbar E, Leykam JF, Kieliszewski MJ. 2001. Contiguous hydroxyproline residues direct hydroxyproline arabinosylation in *Nicotiana tabacum*. *J Biol Chem*. 276:11272–11278.

Shpak E, Leykam JF, Kieliszewski MJ. 1999. Synthetic genes for glycoprotein design and the elucidation of hydroxyproline-*O*-glycosylation codes. *Proc Natl Acad Sci USA*. 96:14736–14741.

Smallwood M, Beven A, Donovan N, Neill SJ, Peart J, Roberts K, Knox JP. 1994.Localization of cell wall proteins in relation to the developmental anatomy of the carrot root apex. *Plant J*. 5:237–246.

Stanley MS, Perry RM, Callow JA. 2005. Analysis of expressed sequence tags from the green alga *Ulva linza* (Chlorophyta). *J Phycol*. 41:1219–1226.

Stortz CA, Cerezo AS. 2000. Novel findings in carrageenans, agaroids and "hybrids" red seaweed galactans. *Curr Top Phytochem*. 4:121–134.

Suzuki S, Li L, Sun YH, Chiang VL. 2006. The cellulose synthase gene superfamily and biochemical functions of xylem-specific cellulose synthase-like genes in *Populus trichocarpa*. *Plant Physiol.* 142:1233–1245.

Tan L, Leykam JF, Kieliszewski MJ. 2003. Glycosylation motifs that direct arabinogalactan addition to arabinogalactan-proteins. *Plant Physiol*. 132:1362–1369.

Thompson EW, Preston RD. 1967. Proteins in the cell walls of some green algae. *Nature*. 213:684–685.

Uehara T, Takeshita M, Maeda M. 1992. Studies on anticoagulant-active arabinan sulfates from the green alga, *Codium latum*. *Carbohydr Res*. 23:309–311.

Van Hengel AJ, Roberts K. 2003. Atagp30, an arabinogalactan-protein in the cell walls of the primary root, plays a role in root regeneration and seed germination. *Plant J*. 36:256–270.

Wood PJ, Fulcher RG, Stone BA. 1983. Studies on the specificity of interaction of cereal cell wall components with Congo red and Calcoflour. Specific detection and histochemistry of (1→3, 1→4)-β-D-glucan. *J Cer Sci*. 1:95–110.

Yariv J, Rapport MM, Graf L. 1962. The interaction of glycosides and saccharides with antibody to the corresponding phenylazo glycoside. *Biochem J*. 85:383–388.

Yates EA, Valdor JF, Haslam SM, Morris HR, Dell A, Mackie W, Knox JP. 1996. Characterization of carbohydrate structural features recognized by anti-arabinogalactan-protein monoclonal antibodies. *Glycobiol*. 6:131–139.

Youngs HL, Gretz MR, West JA, Sommerfield MR. 1998. The cell wall chemistry of *Bangia atropurpurea* (Bangiales, Rhodophyta) and *Bostrychia moritziana* (Ceramiales, Rhodophyta) from marine and freshwater environments. *Phycol Res*. 46:63–73.

Yuasa K, Toyooka K, Fukuda H, Matsuoka K. 2005. Membrane-anchored prolyl hydroxylase with an export signal from the endoplasmic reticulum. *Plant J*. 41:81–94.

Zablackis E, Huang J. 1995. Characterization of the cell-wall polysaccharides of *Arabidopsis thaliana* leaves. *Plant Physiol*. 107:1129–1138.